Journal of South American Earth Sciences 31 (2011) 279–297

Contents lists available at ScienceDirect

Journal of South American Earth Sciences

journal homepage: www.elsevier.com/locate/jsames

High T/P evolution and metamorphic ages of the migmatitic basement of northern Sierras Pampeanas, Argentina: Characterization of a mid-crustal segment of the Famatinian belt

Mariano A. Larrovere [a,b,*], Camilo R. de los Hoyos [c], Alejandro J. Toselli [c], Juana N. Rossi [c], Miguel A.S. Basei [d], Mauricio E. Belmar [e]

[a] Departamento de Geociencias, CRILAR-CONICET, Entre Ríos y Mendoza s/n, 5301 – Anillaco, La Rioja, Argentina
[b] Universidad Nacional de La Rioja, Av. Dr. René Favaloro, 5300 – La Rioja, Argentina
[c] INSUGEO-CONICET, Miguel Lillo 205, 4000 – San Miguel de Tucumán, Argentina
[d] Instituto de Geociencias, Universidade de Sao Paulo, Rua do Lago 562, 05508-080, Sao Paulo, Brazil
[e] Departamento de Geología, Universidad de Chile, Plaza Ercilla 803, 13518 21, Santiago, Chile

ARTICLE INFO

Article history:
Received 21 December 2009
Accepted 15 November 2010

Keywords:
Migmatite
Geothermobarometry
Geochronology
Metamorphism
Sierras Pampeanas
Famatinian orogenic belt

ABSTRACT

New petrologic, thermobarometric and U-Pb monazite geochronologic information allowed to resolve the metamorphic evolution of a high temperature mid-crustal segment of an ancient subduction-related orogen. The El Portezuelo Metamorphic-Igneous Complex, in the northern Sierras Pampeanas, is mainly composed of migmatites that evolved from amphibolite to granulite metamorphic facies, reaching thermal peak conditions of 670–820 °C and 4.5–5.3 kbar. The petrographic study combined with conventional and pseudosection thermobarometry led to deducing a short prograde metamorphic evolution within migmatite blocks. The garnet-absent migmatites represent amphibolite-facies rocks, whereas the cordierite-garnet-K-feldspar-sillimanite migmatites represent higher metamorphic grade rocks. U-Pb geochronology on monazite grains within leucosome record the time of migmatization between ≈477 and 470 Ma. Thus, the El Portezuelo Metamorphic-Igneous Complex is an example of exhumed Early Ordovician anatectic middle crust of the Famatinian mobile belt. Homogeneous exposure of similar paleo-depths throughout the Famatinian back-arc and isobaric cooling paths suggest slow exhumation and consequent longstanding crustal residence at high temperatures. High thermal gradients uniformly distributed in the Famatinian back-arc can be explained by shallow convection of a low-viscosity asthenosphere promoted by subducting-slab dehydration.

1. Introduction

Migmatitic rocks are widely distributed in the northwestern and central region of Argentina which belongs to the Sierras Pampeanas metamorphic basement. These partially melted rocks represent middle to lower crustal sections (Brown, 2001; Rudnick and Gao, 2003) developed during orogens. They have implications not only in the magma generation but also in the tectonic strain and the heat transfer developed during the evolution of the continental crust (Sawyer, 1999; and references therein). The El Portezuelo Metamorphic–Igneous Complex in the northern Sierras Pampeanas, is mainly composed of migmatites and therefore constitutes a suitable unit to study high grade metamorphic processes related to the nature of the Early Ordovician orogen from NW Argentina. The Sierras Pampeanas basement was generated during the evolution of three orogenic events (Aceñolaza and Toselli, 1976; Sims et al., 1998; Aceñolaza et al., 2000; Rapela et al., 2001; Höckenreiner et al., 2003; Büttner et al., 2005; Steenken et al., 2008): the Pampean (Late Neoproterozoic – Lower Cambrian), the Famatinian (Upper Cambrian – Lower Devonian) and the Achalian (Middle Devonian – Lower Carboniferous). The Pampean and Famitianian orogens were interpreted to be the result of subduction and continental collision of several terranes along the margin of Gondwana (Ramos et al., 1986; Ramos, 1988; Kraemer et al., 1995; Rapela et al., 1998, 2001). Alternatively, and especially for NW Argentina, these orogens could have been the result of contiguous stages in the evolution of an intracratonic mobile belt along a subduction zone development on the continental margin of Gondwana with subsequent crust thickening and magmatic activity (Lucassen et al., 2000) followed by an extensional high thermal period in the Early Ordovician (Büttner et al.,

* Corresponding author. Fax: +54 3827 494231.
E-mail address: marianlarro@yahoo.com.ar (M.A. Larrovere).

0895-9811/$ – see front matter © 2011 Elsevier Ltd. All rights reserved.
doi:10.1016/j.jsames.2010.11.006

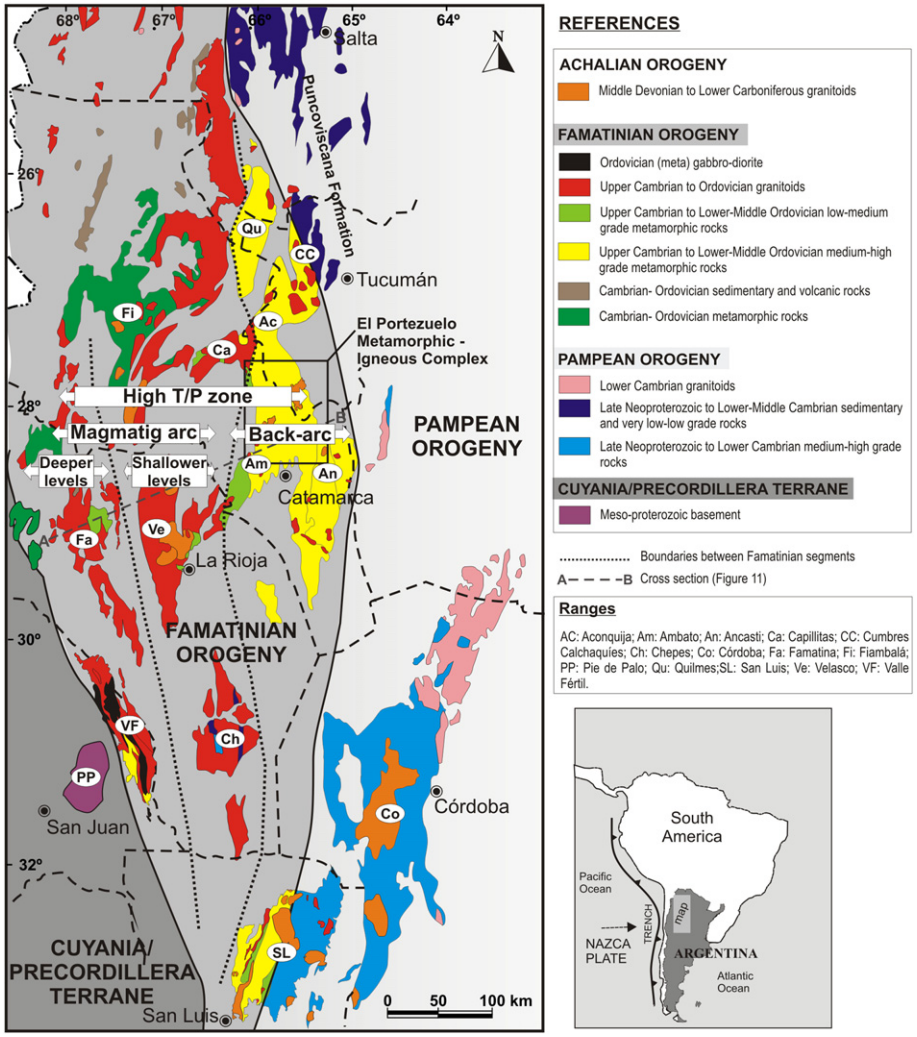

Fig. 1. Generalized sketch map of the Sierras Pampeanas with the main lithologies and relative distribution of Pampean and Famatinian orogenies. A geological setting for the high T/P Famatinian belt is indicated.

2005). The Pampean and Famatinian orogenic belts have been distinguished on the basis of the distribution of magmatic and metamorphic ages based on different isotopic systems (Rapela et al., 2001; and references therein). However, when the distribution of available geochronological data are visualized (e.g. Ramos et al., 2010; Fig. 6) two facts become evident: (1) magmatic ages are much more numerous than metamorphic ones throughout the Sierras Pampeanas; and (2) existing metamorphic ages are clustered within specific areas (e.g. Sierras de Córdoba and San Luis) and they are virtually absent between 27° S and 30° S (e.g. Sierras de Famatina, Velasco, Aconquija, Ambato and Ancasti).

The metamorphic rocks of the basement of the northern Sierras Pampeanas have been correlated with the metamorphic units of Late Neoproterozoic/Cambrian age, which are also related to the Pampean Orogeny in several regional works (Aceñolaza and Toselli, 1981; Aceñolaza and Miller, 1982; Aceñolaza et al., 2000; Rapela et al., 2001, 2007; Steenken et al., 2004, 2008). These latter units were considered as high grade metamorphic equivalents of the low grade Upper Proterozoic/Lower Cambrian metasedimentites of the Puncoviscana Formation (e.g. Aceñolaza and Toselli, 1976). U-Pb metamorphic ages obtained from the north part of the Sierras Pampeanas strongly suggest that the high grade metamorphic basement is Lower Ordovician in age (Büttner et al., 2005). Polymetamorphism has been recorded during the Lower Palaeozoic (Knüver, 1983; Bachmann and Grauert, 1987a,b; Lucassen and Becchio, 2003). Until now there is not data about precise absolute ages and quantitative P-T estimates of the metamorphic rocks from the study area, located between the Ancasti, Ambato and Aconquija ranges in the northern Sierras Pampeanas (Fig. 1). As more chronological and thermobarometric data about metamorphism is gathered, a better understanding of the metamorphic evolution of the Famatinian Orogeny will be accomplished.

The aim of this paper is to report new chronological and thermobarometric data on migmatites of the northern Sierras Pampeanas in order to interpret P-T paths and metamorphic ages for high grade metamorphism of the anatectic middle crust. The results obtained in this research are compared with those of other high thermal crustal terrains of the Famatinian belt in order to deduce a regional geodynamic setting. Thus, this work is a contribution that may be used to understand the tectono-metamorphic evolution of the Sierras Pampeanas during the Ordovician. The new U-Pb ages allowed us to better defining the boundary between the Pampean and Famatinian belts from ≈27 to 29°S in the northern Sierras Pampeanas.

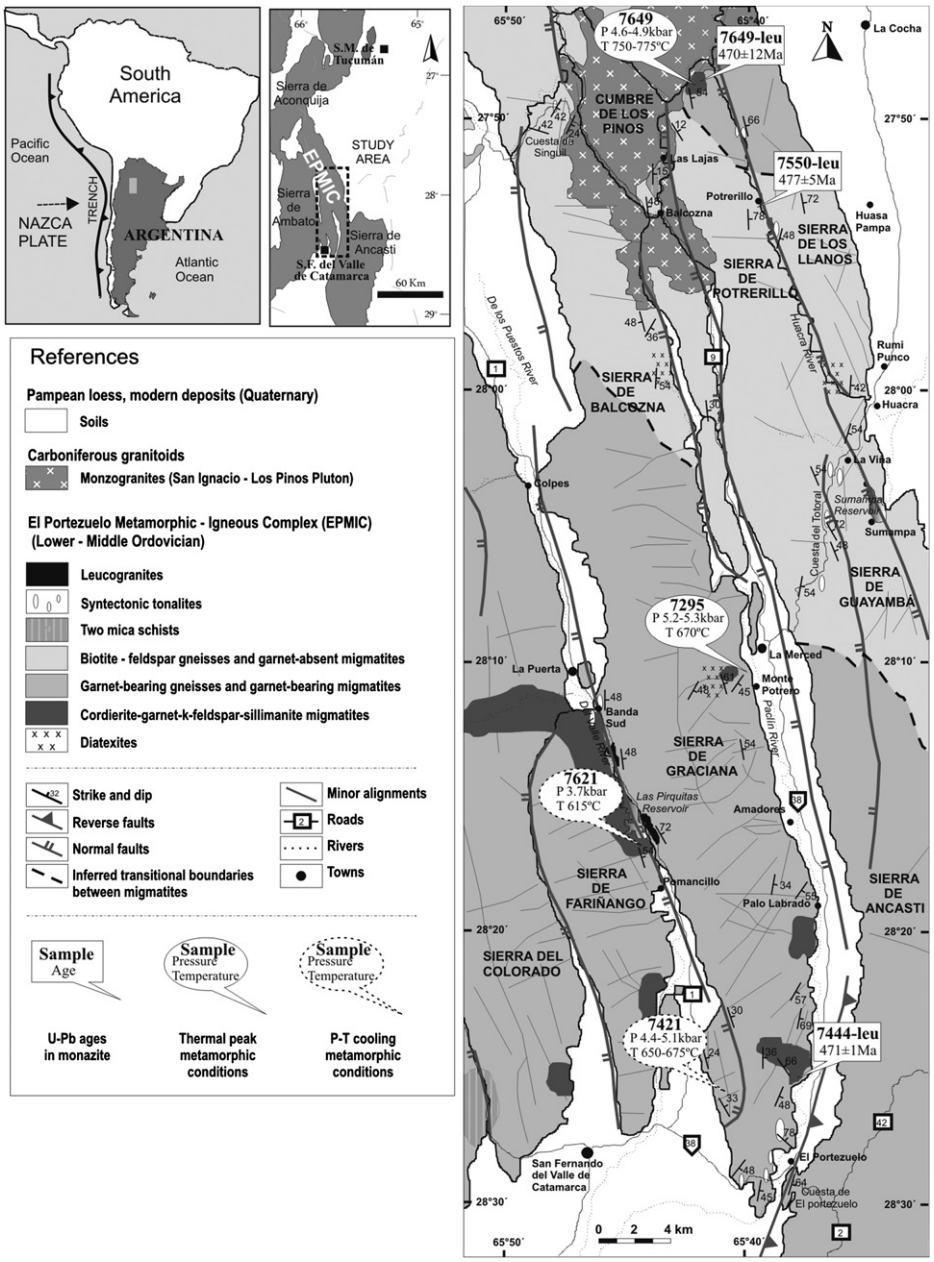

Fig. 2. Geological map of the study area of the northern Sierras Pampeanas including new U-Pb monazite ages and P-T results.

2. Geologic setting of northern Sierras Pampeanas

The Sierras Pampeanas, located in the central and northwestern region of Argentina, are composed almost exclusively of Paleozoic metamorphic and igneous rocks (Fig. 1) formed during the Pampean, Famatinian and Achalian orogens (Aceñolaza and Toselli, 1976; Sims et al., 1998; Aceñolaza et al., 2000; Rapela et al., 2001). The current north-south trending configuration of these ranges is the result of Andean tectonic compression processes (Jordan and Allmendinger, 1986; Ramos et al., 2002). The northern region of the Sierras Pampeanas is made up of several important ranges such as Ancasti, Ambato, Aconquija, Cumbres Calchaquíes, Capillitas and Quilmes, as well as other small ranges (Fig. 1). The basement is dominated by widespread metasedimentary rock sequences metamorphosed under different metamorphic grades, such as granulites, migmatites, gneisses, schists, phyllites, shales, and less abundant marbles, amphibolites, and calcsilicate rocks (Caminos, 1979; Toselli et al., 1986). In the northwest of Argentina the Puncoviscana Formation, extending from the Bolivian border (≈22°S) to the proximities of Tucumán (≈27°S; Toselli, 1990), is formed by thick turbiditic sequences. They were considered to be the sedimentary protolith of higher metamorphic grade rocks of this basement (Aceñolaza and Toselli, 1981; Aceñolaza and Miller, 1982; Willner et al., 1990). Sedimentation and subsequent very low to low grade metamorphism of the Puncoviscana Formation took place during Late Neoproterozoic - Lower Cambrian (Aceñolaza and Durand, 1986; Lork et al., 1990; Adams et al., 1990). The medium to high metamorphism grade has also been regarded as Lower Palaeozoic in age (Aceñolaza and Toselli, 1977; Knüver, 1983), occurring with the development of the Pampean and Famatinian Orogenies. In the Sierra de Ancasti, this metamorphism is represented by prograde transitional changes from the schists of the

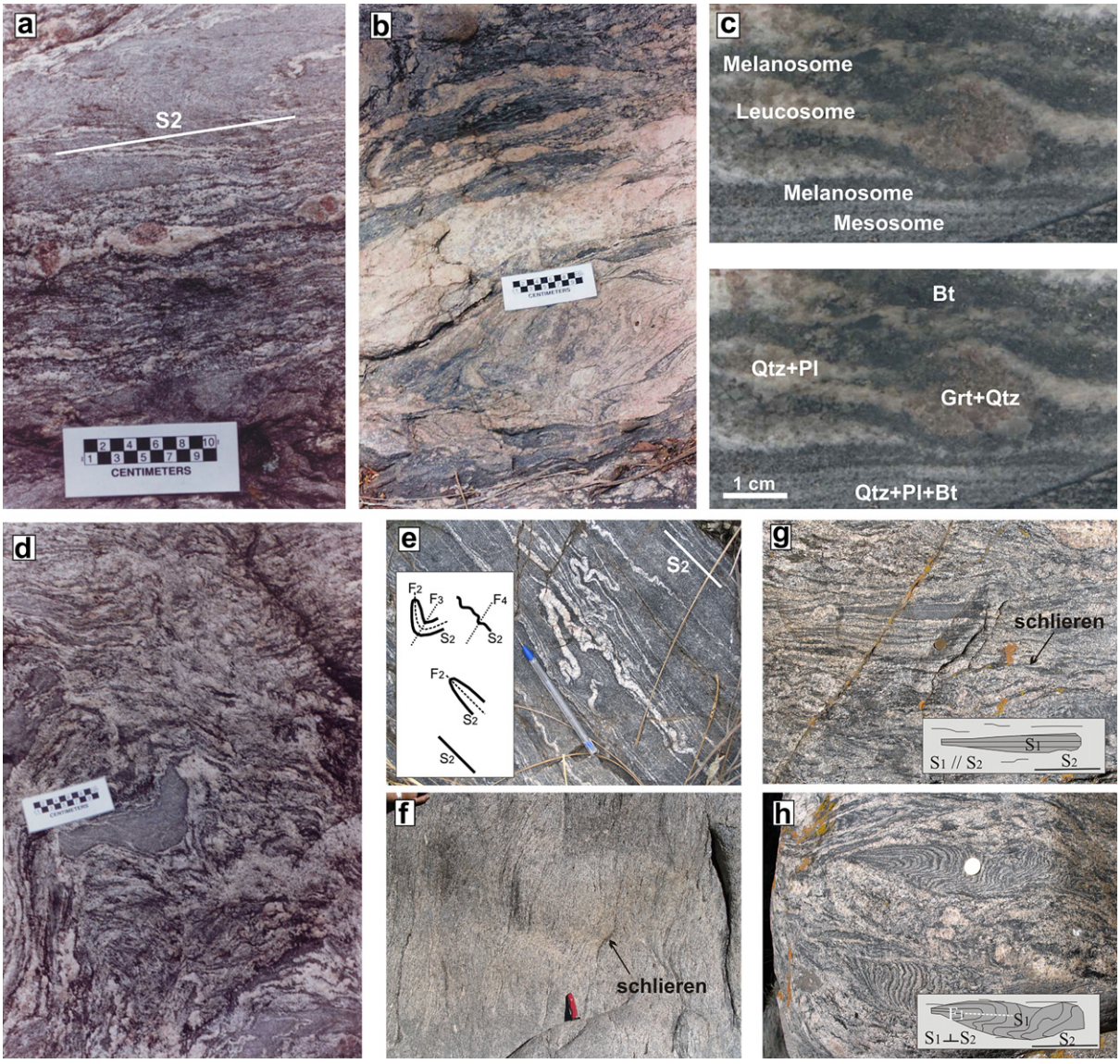

Fig. 3. (a) and (b) Outcrops of well defined banding structure of typical metatexite migmatites of the EPMIC defining a S_2 foliation. (c) Rock polished section showing textural and mineralogical differences between intermediate grey (mesosome) dark (melanosome) and white (leucosome) layers of a stromatitic metatexite. (d) Nebulitic diatexite migmatite including a resister of gneiss (mesosome?) (e) Recognized fold generations affecting the S_2 foliation in a metatexite. (f) Diatexite migmatite with massive texture similar to granitoid rocks. (g) Schlieric diatexite migmatite with abundant biotite schlieren defining a S_2 foliation and evidencing magma flow. Included gneiss resisters with a relict older foliation (S_1) are oriented parallel to S_2. (h) Folded pre-migmatic S_1 foliation in a schlieric diatexite migmatite.

Ancasti Formation to the migmatites of El Portezuelo Formation (Aceñolaza and Toselli, 1977; Willner, 1983; Willner et al., 1983), the latter having reached the cordierite-sillimanite-K-feldspar metamorphic zone related to a low to medium regional metamorphism pressure. Similar metamorphic conditions were inferred on the Sierra de Quilmes (Rossi de Toselli et al., 1987; Büttner et al., 2005). The occurrence of a regional high thermal regime during the evolution of Lower Paleozoic orogenies has been suggested for several ranges of the Sierras Pampeanas (Lucassen and Becchio, 2003; Lucassen and Franz, 2005; Otamendi et al., 2008).

Granitoid rocks intruded the metamorphic basement from the Ordovician to the Carboniferous. The magmatic activity in the study area and nearby ranges can be enclosed in two major events: Lower - Middle Ordovician (Famatinian) and Late Devonian - Early Carboniferous (Achalian). The former and more important is characterized by the Capillitas Batholith, the main granitoid body that crops out in the area and is representative of the Ordovician peraluminous S-type Famatinian magmatism (Toselli et al., 1996; Pankhurst et al., 2000; Rossi et al., 2002). In addition, several coeval I-type and S-type plutons complete the Ordovician magmatic groups (Knüver, 1983; Toselli, 1992; Rapela et al., 2005; Büttner et al., 2005). On the other hand, the Devonian - Carboniferous magmatism in the area is restricted to discordant bodies of not well constrained genesis and age (Knüver, 1983; Toselli, 1983, 1992; Indri and Barber, 1987).

Ductile NNW-SSE trending shear zones affecting Famatinian and older rocks have been identified in several areas (Le Corre and Rossello, 1994; Larrovere et al., 2008), but the age of shearing remains uncertain. Mylonitic events in northern Sierras Pampeanas probably took place between the Upper Ordovician and the Lower Devonian (López et al., 2000; Höckenreiner et al., 2003). In other areas of the northern Sierras Pampeanas, undeformed carboniferous granites cross-cut the mylonitic shear zones (e.g. Grosse et al., 2009 and references therein) constraining the minimum age of mylonitization.

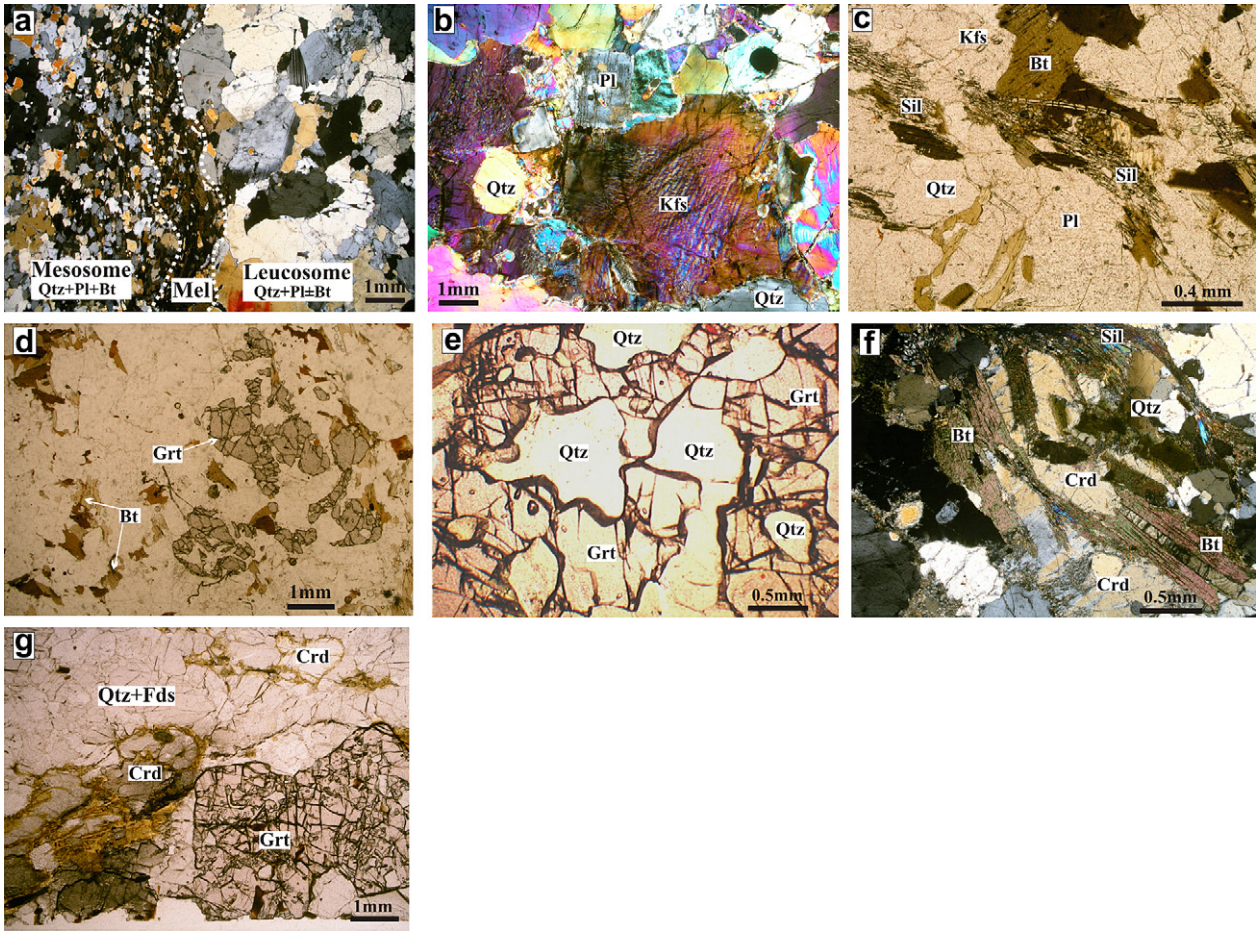

Fig. 4. (a) Micro-scale structure in a stromatitic-type metatexite showing textural differences between the three structural parts: mesosome, melanosome and leucosome. (b) Medium to coarse grained leucosome with igneous-like texture in a garnet-absent migmatite. Plagioclase shows crystals faces reflecting crystallization in a melt. (c) Qtz + Pl + Bt + Kfs + Sil mineral assemblage in diatexites of the garnet-absent migmatites. (d) Garnet clusters in a diatexite of the garnet-bearing migmatites coexisting with biotite. (e) Interlobate association of garnet and quartz in leucosomes of the garnet-bearing migmatites interpreted as a prograde microestructure associated with melting. (f) Equilibrium Crd-Sil-Bt assemblage in a leucosome of the cordierite-garnet-K-feldspar-sillimanite migmatites. (g) Garnet coexisting with cordierite in a quartz-feldspar rich matrix of a leucosome of the cordierite-garnet-K-feldspar-sillimanite migmatites.

3. El Portezuelo Metamorphic-Igneous Complex

The El Portezuelo Metamorphic-Igneous Complex (EPMIC) is a wide metasedimentary unit defined into several small ranges localized in the northern Sierras Pampeanas, between the ranges of Ancasti, Ambato and Aconquija (Figs. 1 and 2). The EPMIC is mainly composed of migmatites but also has gneisses, schists and syntectonic tonalites. Subordinate marbles and calcsilicate rocks are also present. The EPMIC derives from protoliths that consist of lithic wacke, pelitic and minor calcareus rocks. The migmatites are mostly stromatitic–type metatexites, but also diatexites have been recognized, which define a regional N-S migmatitic belt. Lithologic continuity has been observed between migmatites, gneisses and schists. Therefore, rocks of both the lowest metamorphic grade (schists) and the highest metamorphic grade (migmatites) are considered to be from the same continental crust block but developed in different structural levels or under distinct thermal regime. Metamorphic rocks of the EPMIC are the product of a regional metamorphic event M_2. Metatexites show an extensive development of leucosomes parallel to the pre-migmatization foliation. A banding structure is formed by intermediate grey (mesosome), dark (melanosome), and white (leucosome) layers (Fig. 3a,b). The neoformed portion of metatexites has thin (1–4 mm) and biotite-rich melanosomes, and quartz–feldspar coarsely grained leucosomes (Figs. 3c and 4a) ranging from 0.5 to 20 cm thick. In areas where the melt fraction increased and it was retained (Sawyer, 1999) diatexites have been observed. Diatexites are coarsely grained and present a massive texture similar to granitoid rocks (Fig. 3f). Schlieric diatexite migmatites, nebulitic diatexite migmatites and diatexite migmatites (Sawyer, 2008) were recognized (Fig. 3d,f,g,h). Biotite schlieren evidencing magma flow are common (Fig. 3f,g, Millord and Sawyer, 2003) as well as frequent leucocratic bands and pockets. Generally, boundaries between diatexites and metatexites are transitional. Garnet-, sillimanite-, and biotite-feldspar-gneisses are interfringered within migmatite domains. A textural and mineralogical transition between migmatites, two mica gneisses and two mica schists are common. Several igneous bodies are generally present within deeper rock domains (migmatites) of the EPMIC. They are small bodies composed of medium-grained equi-granular tonalites concordant with the host-rock.

A regional S_2 foliation defined by the mesosome-melanosome-leucosome layering in metatexites is present in the migmatites with a NNW-SSE/N-S strike and ENE/E dip. The S_2 foliation is recognized also in the diatexites, where it is mainly defined by biotite schlieren parallel to the metatexite layering. This S_2 foliation continues in the different basement blocks as well as in the lower metamorphic grade rocks of the EPMIC, where it is defined by differentiated layering. Locally, a S_3 foliation of ductile syn-migmatic origin cuts

the S_2 foliation. The anatectic melts presents in the S_2 foliation (metatexite layering) fill dilatant spaces (low pressure sites) and define the S_3 foliation. A relict older foliation (S_1) is preserved within resisters of schists and gneisses included in leucosomes and diatexites (Fig. 3d,g,h). Folding of the S_1 foliation generates F_1 folds. Three generations of folds (F_2, F_3 and F_4) affect the S_2 foliation (Fig. 3e). F_2 folds are tight and intrafolial with hinges parallel to S_2. F_3 folds appear re-folding F_2 and both are probably coeval with the development of cm-scale F_4 folds that affect the S_2 foliation. In the migmatites, the main S_2 foliation would be related to the S_3 axial planar schistosity in the migmatites of the Sierra de Ancasti which correspond to the D_3 deformational phase (Miller and Willner, 1981).

Although the Portezuelo Metamorphic-Igneous Complex was defined for an enclosed area of northern Sierras Pampeanas (Larrovere, 2009), this unit would span the basement rocks of the nearby ranges of Ancasti, Ambato and Aconquija.

4. Petrography: textures and mineral assemblages of migmatites

In the EPMIC we recognize three broad migmatite groups characterized by distinctive mineral assemblages and classified as follow: garnet-absent migmatites, garnet-bearing migmatites and cordierite-garnet-K-feldspar-sillimanite migmatites. Both metatexites and diatexites are present in all groups.

4.1. Garnet-absent migmatites

Migmatites in this group are composed almost exclusively of quartz, feldspar and biotite. Sillimanite is scarce, and garnet and cordierite are totally absent. Metatexites have fine grained mesosomes formed by quartz, plagioclase and biotite (Fig. 4a). Oriented biotites and elongated quartz and plagioclase crystals define a metamorphic foliation (S_2). K-feldspar, fibrolite and muscovite are occasionally present. Retrograde fibrolite occurs replacing both kinds of micas, whereas retrograde muscovite grows cutting the S_2 main foliation. Accessory mineral phases, such as apatite, zircon and opaque minerals are common in mesosomes, melanosomes and leucosomes. Dark medium grained melanosomes, of 1–2 mm thick, mostly contain well aligned platy biotite and also less abundant quartz and plagioclase. Scarce muscovite and fibrolite of retrograde origin appear in melanosomes and leucosomes. A relic quartz-plagioclase-biotite mesosome mineral assemblage is sporadically observed within melanosomes. The medium to coarse grained leucosomes which have igneous-like texture mainly contain quartz, plagioclase and K-feldspar. The leucosomes are nearly absent of biotite, and plagioclase is more abundant than K-feldspar; the latter mineral is not always present. Some plagioclase shows crystals faces (Fig. 4b) reflecting crystallization in a melt (Vernon, 2004 and references therein). A typical leucosome mineral assemblage in garnet-absent migmatites is Qtz + Pl + Bt ± Kfs (symbols after Siivola and Schmid, 2007). Some small bodies of sillimanite-rich diatexites occur associated to metatexites. The abundance of sillimanite and a higher grade of melting in diatexites related to nearby metatexites suggest that diatexites originated from more pelitic precursors. The diatexites (sample 7551) contain quartz, plagioclase, K-feldspar, biotite and sillimanite. Diatexites have igneous-like texture, with anhedral quartz, plagioclase and K-feldspar, as well as with subhedral biotite and prismatic sillimanite that is poorly aligned (Fig. 4c). The mineral assemblage Qtz + Pl + Bt + Kfs + Sil, the total absence of muscovite, and the occurrence of rocks that underwent partial melting indicate that the migmatization occurred probably by the reaction (Huang and Wyllie, 1974; Spear et al., 1999):

$$\text{muscovite} + \text{quartz} \rightarrow \text{sillimanite} + \text{K} - \text{feldspar} + \text{melt} \quad (1)$$

4.2. Garnet-bearing migmatites

This migmatite group is characterized by the occurrence of garnet in leucosomes, whereas mesosomes and melanosomes are generally garnet free. No significant mineral and textural differences are found between garnet-bearing migmatites and garnet-absent migmatites metatexite mesosomes. Mesosomes in garnet-bearing migmatites contain quartz, plagioclase and biotite. Poikiloblastic garnet occasionally appears as isolated and elongated grains, with inclusions of quartz and biotite. Melanosomes are thin, medium grained, biotite-rich bands with lepidoblastic texture. Minor amounts of lengthened quartz and plagioclase also appear. Garnet is rarely observed, generally idioblastic and sometimes containing inclusions of quartz, biotite and opaque minerals. Zircon, apatite and opaque minerals are the dominant accessory minerals in mesosomes and melanosomes. Leucosomes have igneous-like texture and are formed by quartz, plagioclase, garnet, biotite and K-feldspar; the latter does not always occur. Minerals in leucosomes can be slightly aligned, with quartz presenting subgrains. Garnet is idiomorphic to subidiomorphic, and in some leucosomes and diatexites it tends to amalgamate forming garnet-clusters (Fig. 4d). In some cases amoeboid garnet occurs associated with lobate quartz grains (Fig. 4e). The interlobate association of garnet and quartz in leucosomes has been interpreted as a prograde microstructure associated with melting (Waters, 2001). Plagioclase, biotite, and oval quartz are common inclusions within garnet. The garnets in the leucosomes are bigger than garnets in melanosomes and mesosomes. The general mineral assemblage for leucosome of garnet-bearing migmatites is Qtz + Pl + Bt + Grt ± Kfs. The prograde reaction responsible for generating garnet-bearing leucosomes is deduced to be reaction (Vielzeuf and Montel, 1994):

$$\text{biotite} + \text{quartz} + \text{plagioclase} \rightarrow \text{garnet} \pm \text{K} - \text{feldspar} + \text{melt} \quad (2)$$

The observed inclusions of quartz, plagioclase and biotite within poikilitic garnets indicate that these minerals were the probable reactant phases in the garnet growth. Since sillimanite is absent in garnet migmatites, probably a dioctahedral Al component in biotite makes up the sillimanite discrete phase to stabilize this reaction (Patiño Douce et al., 1993; Otamendi et al., 1999).

4.3. Cordierite-garnet-K-feldspar-sillimanite migmatites

This group differs mineralogically from the other migmatite groups since it contains cordierite and higher amounts of sillimanite and K-feldspar. These mineral phases predominantly appear in leucosomes and diatexites. In metatexites, mesosomes are finely-grained, markedly foliated, and contain quartz, plagioclase and biotite. Platy biotites and elongated quartz and plagioclases define the main foliation. Cordierite and sillimanite are sometimes present. Sillimanite occurs in two forms: within quartz, plagioclase, and cordierite as small needle-like crystals; or intergrown with biotite. Cordierite is anhedral, with cracked crystal edges, and inclusions of quartz, biotite, zircon, apatite and sillimanite. Melanosome biotite-rich bands reach 1–4 mm width. They also contain quartz and plagioclases, and occasionally cordierite, sillimanite and garnet. Needle-like sillimanite intergrows with biotite. Anhedral cordierite is commonly associated with biotite. Garnet occurs as isolated, elongated or rounded grains, with inclusions of biotite and quartz. The leucosomes are medium to coarse grained, have igneous-like texture and mainly contain quartz, plagioclase, K-feldspar, biotite, sillimanite, cordierite and garnet. Accessory mineral phases such as apatite, zircon, monazite and opaque minerals are common. Lath-like crystals of sillimanite are intergrown with biotite and cordierite (Fig. 4f). Sillimanite also

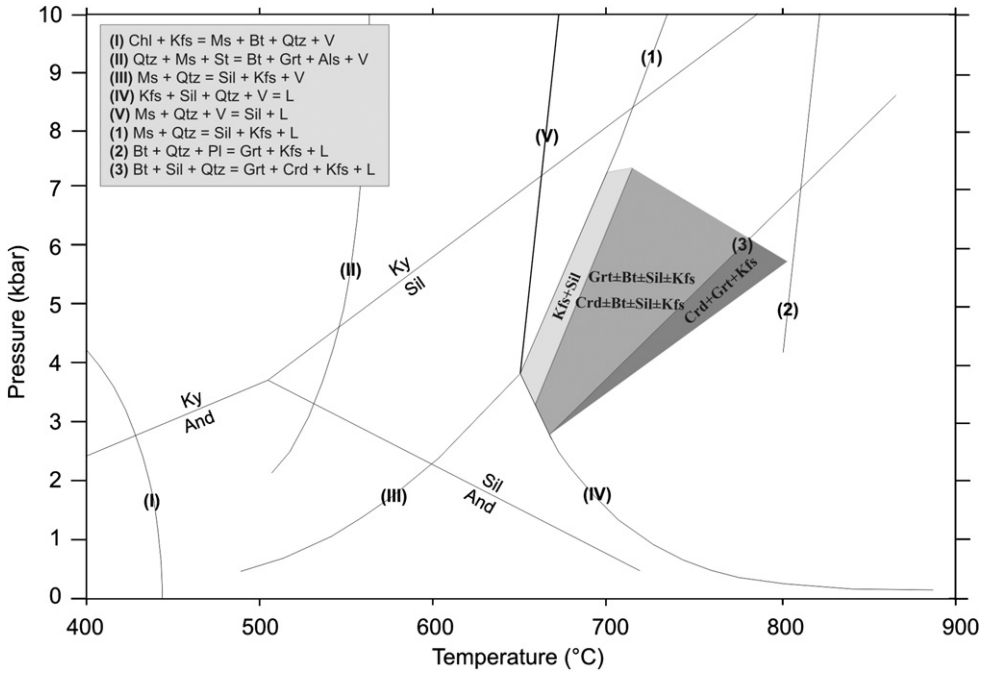

Fig. 5. P–T diagram showing relative metamorphic peak conditions of migmatites derived from petrological observations. Reactions I: Simpson et al. (2000); II: from Yardley (1989); III and 3: Spear et al. (1999); IV, V, and 1: Huang and Wyllie, 1974; 2: Vielzeuf and Montel (1994). Aluminosilicate phase diagram from Holdaway (1971). V: vapor, L: liquid (melt).

appears as clusters of several crystals oriented in different directions or as small needles included within cordierite. Retrograde fibrolite is present in cordierite boundaries. Large cordierite grains are anhedral, with amoeboid and oval shapes, and frequently altered by chlorite, pinnite or white mica. The garnets are subhedral and with diameters that reach 1 cm. They are normally poikiloblastic with inclusions of biotite, quartz and plagioclase, although some of them are inclusion-free. The mineral assemblage for the leucosome is Qtz + Pl + Crd ± Bt ± Kfs ± Sil ± Grt. In some leucosomes and diatexites, slightly different textural and compositional domains can be recognized, thus different mineral assemblages are observed. Commonly a biotite-rich domain with Qtz + Pl + Bt + Grt + Sil and a cordierite-rich light-coloured domain with Qtz + Pl + Kfs + Bt + Crd + Sil are identified. In the latter domain, also a Qtz + Pl + Bt + Kfs + Grt + Crd assemblage appear coexisting (Fig. 4g). Isolated cordierite grains in a quartz-feldspar matrix are frequent. The possible melt-forming reactions including cordierite as product mineral phase could be (Spear et al., 1999; Otamendi et al., 2008):

$$\text{biotite} + \text{sillimanite} + \text{quartz} \rightarrow \text{garnet} + \text{cordierite} + \text{K} - \text{feldspar} + \text{melt} \quad (3)$$

$$\text{biotite} + \text{sillimanite} + \text{quartz} + \text{plagioclase} \rightarrow \text{cordierite} + \text{K} - \text{feldspar} + \text{melt} \quad (4)$$

$$\text{biotite} + \text{sillimanite} + \text{quartz} + \text{plagioclase} \rightarrow \text{garnet} + \text{cordierite} + \text{K} - \text{feldspar} + \text{melt} \quad (5)$$

The observed mineral assemblages allow predicting metamorphic conditions (Fig. 5) within the stability field defined by reactions (1) and (3). The mineral assemblages Qtz + Pl + Kfs + Bt + Crd + Sil and Qtz + Pl + Bt + Grt + Sil fall in this stability field, whereas the Qtz + Pl + Bt + Kfs + Grt + Crd assemblage indicates that the metamorphic conditions defined by reaction (3) were reached. The cordierite + garnet + K-feldspar assemblage is typical of high grade migmatites and is often taken to mark the beginning of the granulite facies (Yardley, 1989). It should be noted that the garnet-bearing migmatite group may have originated at higher temperature according to the general reaction of Vielzeuf and Montel (1994) obtained from melting experiments of metagreywackes.

5. Geothermobarometry

Temperatures and pressures were calculated using single analysis from minerals in contact with each other. Multiphase equilibria method was applied using the software TWQ (Berman, 1991) version 2.3 edition 2.32. TWQ contains internally consistent thermodynamic data as well as solid solution data, which ensure the quality of thermobarometric results. Thermodynamic data and activity models correspond to files DEC06.DAT and DEC06.SLN respectively. The garnet solution model of Berman and Aranovich (1996) is used with revised Mn–Mg–Fe mixing properties in the version 2.32. For biotite, solubility data between Al, Fe and Mg of Berman et al. (2007) are used. For plagioclase, the Al − avoidance model of Fuhrman and Lindsley (1988) is utilized. Moreover conventional geothermobarometry was applied to test the results obtained with TWQ. The garnet-biotite geothermometer with the calibration of Holdaway (2000) and the garnet-biotite-plagioclase-quartz (GBPQ) geobarometer of Wu et al. (2004) are used. Assumed pressures required for the thermometer were taken from calculations using the TWQ software. The obtained temperatures were used for conventional barometry. Regarding activity models (activity–composition relations), the GBPQ geobarometer uses models of Holdaway (2000) for biotite and garnet, and the model of Fuhrman and Lindsley (1988) for plagioclase. Na-in-cordierite thermometry with the calibrations of Wyhlidal et al. (2007) and Mirwald et al. (2008) for low X_{H2O} was also used.

P-T pseudosections were applied using the PERPLE-X software package (Connolly, 1990). Pseudosections were used to estimate P-T

Table 1
Bulk major compositions used in pseudosections.

Rock	Diatexite	Leucosome
Sample	7551	7649-leu
SiO_2	69.79	74.70
Al_2O_3	13.93	11.85
Fe_2O_3 (total)	4.67	3.13
FeO	4.20	2.81
MnO	0.07	0.07
MgO	1.92	1.48
CaO	1.53	0.84
Na_2O	2.19	1.82
K_2O	3.31	3.18
TiO_2	0.62	0.26
P_2O_5	0.28	0.10
LOI	1.09	0.83
Total	99.39	98.24

Note: FeO = Fe_2O_3 (total) × 0.899.
FeO is not considered for the total.

conditions from reconstruction of stability fields of theoretical assemblages and comparison to observed mineral assemblages. The internally consistent thermodynamic database of Holland and Powell (1998) was used. For pseudosection calculations Fe_2O_3 total was corrected to FeO stoichiometrically and loss on ignition (LOI) was assumed to represent the H_2O bulk content (Table 1).

To determine P-T conditions of the metamorphism (M2) that produced the widespread anatexis of metasedimentary rocks of the EPMIC five samples of migmatites were selected. The chosen samples were: 7295 and 7421 (garnet-bearing migmatites group) from NE and SW of the Sierra de Graciana respectively, samples 7649 (cordierite-garnet-K-feldspar-sillimanite migmatites) and 7551 (garnet-absent migmatites) from north and central of the Sierra de Potrerillo respectively, and sample 7621 (cordierite-garnet-K-feldspar-sillimanite migmatites) from east of the Sierra de Fariñango (Fig. 2). We evaluated all migmatite groups in order to establish probable different metamorphic P-T conditions reached during the evolution of each group.

5.1. Garnet-absent migmatites

Sample 7551 is a schlieric diatexite with mineral assemblage Qtz + Pl + Bt + Kfs + Sil. Due to lack of suitable mineral phases to apply conventional thermobarometry, we constructed pseudosections to compare between theoretical and observed mineral assemblages in order to roughly estimate P-T conditions. A stability field was calculated for the theoretical assemblage Bt + melt + Pl + Sil + Kfs + Qtz which is in agreement with the observed mineral assemblage (Fig. 6a). This field is wide for pressures, whereas the range of temperatures is relatively narrow at low-medium pressures. Assuming a mean pressure of around 5 kbar from thermobarometry as estimated in the other samples (see below), the stability field is within the range of 675–730 °C. The pseudosection allows deducing the gradual mineral changes during the metamorphic prograde evolution of the rock. For pressures of ≈5 kbar, the pseudosection predicts that melting started at around 670 °C. The prograde mineral assemblages with cordierite appear at 730 °C after the Bt + melt + Pl + Sil + Kfs + Qtz stability field, whereas coexisting garnet and cordierite are stable from 750 °C. Taking this latter temperature, cordierite disappears at pressures above 5.3 kbar and garnet remains stable.

5.2. Garnet-bearing migmatites

Sample 7295 is a migmatite with leucosome assemblage Qtz + Pl + Bt + Grt. Plagioclase is oligoclase with compositions $Ab_{70-72}An_{28-27}Or_2$ (Table 2); biotite has Ti contents from 0.12 to

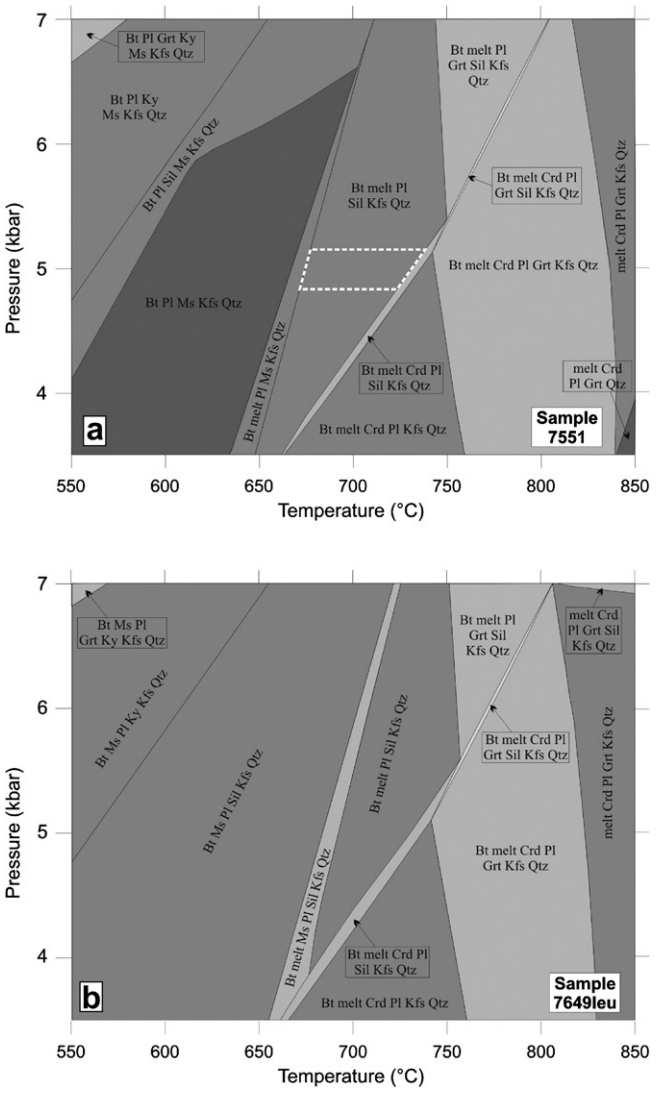

Fig. 6. (a) P-T pseudosection modelled for Qtz + Pl + Bt + Kfs + Sil diatexite of the garnet-absent migmatites. The white dashed area represents probable peak metamorphic conditions within the stability field calculated for the theoretical assemblage Bt + melt + Pl + Sil + Kfs + Qtz, which is in agreement with the observed mineral assemblage. (b) P-T conditions of different mineral assemblages predicted by pseudosections of the cordierite-garnet-K-feldspar-sillimanite migmatites.

0.17 pfu and with X_{Mg} ranging from 0.50 to 0.54; garnet is almandine with compositions $Alm_{69-72}Grs_{3-4}Prp_{16-20}Sps_{6-9}$. In general, garnet has a compositionally flat zoning pattern (Fig. 7a,b), typical of garnets that underwent diffusion processes at high grade conditions (Yardley, 1977). Only some garnets show little variations with a spessartine component increasing rimward whereas pyrope decreases, leading to a drop in X_{Mg}. We calculated P-T conditions of ≈670 °C and 5.2–5.3 kbar on core analysis (Table 3, Fig. 8a), and ≈620–640 °C and 4.8–5.1 kbar on rim analysis using multiphase equilibria method (intersection of two independent mineral reactions: GASP and Grt-Bt). Since the mineral assemblage is absent of sillimanite and assuming that the activity of Al_2SiO_5 = 1, GASP determinations should be considered as maximum pressure calculated (Ghent and Grover, 1995). The presence of sillimanite in nearby rocks in the area permits to suppose that the leucosomes evolved within the sillimanite stability field. We tested the results, applying the conventional Grt-Bt thermometer and GBPQ geobarometer, which are useful for sillimanite absent mineral

Table 2
Representative mineral chemical analyses used in thermobarometric calculations.

Sample	7295		7421	7621		7649			
Migmatite group	G-Mig	G-Mig	G-Mig	CGKfS-Mig	CGKfS-Mig	CGKfS-Mig	CGKfS-Mig	CGKfS-Mig	CGKfS-Mig
Mineral	Garnet	Garnet	Garnet	Garnet	Garnet	Garnet	Garnet	Garnet	Garnet
Mineral remarks	Core	Rim	Rim	Mid	Rim	Inn-core	Out-core	Out-rim	Inn-rim
No. of O: 24									
SiO_2	37.67	39.10	38.68	38.18	37.72	38.61	38.21	39.37	38.06
TiO_2	0.07	0.09	0.00	0.07	0.00	0.00	0.27	0.10	0.02
Al_2O_3	22.00	21.34	21.88	21.86	21.49	22.58	22.35	22.38	22.73
FeO	30.14	29.27	26.97	30.12	30.61	28.22	27.74	25.36	27.80
MnO	3.10	3.76	6.04	3.51	3.76	6.44	6.03	8.37	7.82
MgO	4.93	3.85	4.60	4.45	4.02	4.93	4.68	3.05	4.34
CaO	1.13	1.24	1.09	1.07	0.99	0.93	0.94	1.31	1.03
Na_2O	0.00	0.23	0.03	0.28	0.00	0.00	0.30	0.00	0.16
Total	99.04	98.88	99.29	99.54	98.59	101.71	100.52	99.94	101.96
Si	6.04	6.48	6.29	6.13	6.17	6.03	6.04	6.49	5.90
Ti	0.01	0.01	0.00	0.01	0.00	0.00	0.03	0.01	0.00
Al	4.16	4.17	4.19	4.14	4.14	4.16	4.17	4.35	4.15
Fe_2	4.04	4.06	3.66	4.05	4.19	3.69	3.67	3.50	3.60
Mg	1.18	0.95	1.11	1.07	0.98	1.15	1.10	0.75	1.00
Ca	0.19	0.22	0.19	0.18	0.17	0.16	0.16	0.23	0.17
Mn	0.42	0.53	0.83	0.48	0.52	0.85	0.81	1.17	1.03
Na	0.00	0.07	0.01	0.09	0.00	0.00	0.09	0.00	0.05
Xgrossular	0.03	0.04	0.03	0.03	0.03	0.03	0.03	0.04	0.03
Xpyrope	0.20	0.16	0.19	0.18	0.17	0.20	0.19	0.13	0.17
Xalmandine	0.69	0.70	0.63	0.69	0.71	0.63	0.63	0.62	0.62
Xspessartine	0.07	0.09	0.14	0.08	0.09	0.15	0.14	0.21	0.18
XMg	0.23	0.19	0.23	0.21	0.19	0.24	0.23	0.18	0.22

Sample	7295			7421		7621		7649		
Migmatite group	G-Mig	G-Mig	G-Mig	G-Mig	G-Mig	CGKfS-Mig	CGKfS-Mig	CGKfS-Mig	CGKfS-Mig	CGKfS-Mig
Mineral	Biotite	Biotite	Biotite	Biotite	Biotite	Biotite	Biotite	Biotite	Biotite	Biotite
Mineral remarks	Core	Rim	Rim	Rim-mtx	Rim-mtx	Core	Rim	Core	Core	Rim
No. of O: 11										
SiO_2	35.97	36.61	36.19	35.51	35.57	35.17	35.58	36.45	35.63	36.98
TiO_2	2.74	2.68	2.75	2.48	2.60	2.49	2.99	3.07	3.55	2.98
Al_2O_3	18.51	18.25	18.69	20.35	20.30	19.90	19.86	19.07	19.02	19.72
FeO	16.15	16.49	15.44	15.86	14.52	15.74	16.06	19.41	19.05	18.53
MnO	0.23	0.14	0.08	0.13	0.24	0.02	0.06	0.87	0.34	0.27
MgO	10.10	9.17	9.86	9.76	9.71	10.54	10.03	8.72	9.11	8.95
CaO	0.22	0.38	0.25	0.00	0.02	0.01	0.01	0.23	0.13	0.31
Na_2O	0.00	0.37	0.66	0.00	0.19	0.12	0.00	0.18	0.15	0.10
K_2O	9.26	9.23	9.39	10.40	9.91	10.01	9.64	8.96	9.90	7.85
Total	93.18	93.32	93.31	94.49	93.06	94.00	94.23	96.96	96.88	95.69
Si	2.75	2.80	2.76	2.69	2.71	2.67	2.69	2.72	2.67	2.75
Al_T	1.25	1.20	1.24	1.31	1.29	1.33	1.31	1.28	1.33	1.25
Ti	0.16	0.15	0.16	0.14	0.15	0.14	0.17	0.17	0.20	0.17
Al_O	0.42	0.45	0.44	0.50	0.54	0.46	0.46	0.40	0.35	0.48
Fe_2	1.03	1.06	0.99	1.00	0.93	1.00	1.02	1.21	1.20	1.15
Mn	0.01	0.01	0.01	0.01	0.02	0.00	0.00	0.06	0.02	0.02
Mg	1.15	1.05	1.12	1.10	1.10	1.19	1.13	0.97	1.02	0.99
Ca	0.02	0.03	0.02	0.00	0.00	0.00	0.00	0.02	0.01	0.02
Na	0.00	0.05	0.10	0.00	0.03	0.02	0.00	0.03	0.02	0.01
K	0.90	0.90	0.91	1.00	0.96	0.97	0.93	0.85	0.95	0.75
XMg	0.53	0.50	0.53	0.52	0.54	0.54	0.53	0.44	0.46	0.46

Sample	7295			7421	7621		7649	
Migmatite group	G-Mig	G-Mig	G-Mig	G-Mig	CGKfS-Mig	CGKfS-Mig	CGKfS-Mig	CGKfS-Mig
Mineral	Plagioclase	Plagioclase	Plagioclase	Plagioclase	Plagioclase	Plagioclase	Plagioclase	Plagioclase
Mineral remarks	Core	Core	Rim	Rim-mtx	Core	Rim	Core	Rim
No. of O: 8								
SiO_2	60.92	60.79	60.71	60.93	60.25	60.58	62.24	62.00
TiO_2	0.00	0.08	0.00	0.00	0.02	0.00	0.03	0.08
Al_2O_3	23.47	24.38	23.49	24.66	24.69	24.09	24.78	24.29
Fe_2O_3	0.22	0.22	0.35	0.12	0.17	0.00	0.10	0.24
Mn_2O_3	0.11	0.10	0.00	0.00	0.00	0.00	0.06	0.03
MgO	0.15	0.14	0.04	0.04	0.08	0.05	0.09	0.00

(*continued on next page*)

Table 2 (*continued*).

Sample	7295			7421	7621		7649	
Migmatite group	G-Mig	G-Mig	G-Mig	G-Mig	CGKfS-Mig	CGKfS-Mig	CGKfS-Mig	CGKfS-Mig
Mineral	Plagioclase	Plagioclase	Plagioclase	Plagioclase	Plagioclase	Plagioclase	Plagioclase	Plagioclase
Mineral remarks	Core	Core	Rim	Rim-mtx	Core	Rim	Core	Rim
CaO	5.64	5.64	5.54	5.46	5.98	5.41	4.73	5.22
Na_2O	8.35	7.85	8.29	7.78	7.98	7.99	6.12	5.30
K_2O	0.38	0.35	0.33	0.57	0.24	0.26	0.56	0.44
Total	99.24	99.56	98.75	99.57	99.41	98.38	98.71	97.60
Si	2.733	2.713	2.735	2.717	2.696	2.730	2.766	2.781
Al	1.241	1.282	1.247	1.296	1.302	1.279	1.298	1.284
Fe_3	0.008	0.007	0.012	0.004	0.006	0.000	0.003	0.008
Mn_3	0.004	0.003	0.000	0.000	0.000	0.000	0.002	0.001
Ti	0.000	0.003	0.000	0.000	0.001	0.000	0.001	0.003
Ca	0.271	0.270	0.267	0.261	0.287	0.261	0.225	0.251
Na	0.727	0.679	0.724	0.673	0.692	0.698	0.528	0.461
K	0.022	0.020	0.019	0.032	0.014	0.015	0.032	0.025
XAnorthite	0.266	0.278	0.265	0.270	0.289	0.268	0.287	0.340
XAlbite	0.713	0.701	0.717	0.696	0.697	0.717	0.672	0.625
X K-Feldspar	0.021	0.021	0.019	0.034	0.014	0.015	0.040	0.034

Sample	7621		7649	
Migmatite group	CGKfS-Mig	CGKfS-Mig	CGKfS-Mig	CGKfS-Mig
Mineral	Cordierite	Cordierite	Cordierite	Cordierite
Mineral remarks	Rim	Core	Core	Core
No. of O: 18				
SiO_2	48.43	47.72	46.91	48.63
TiO_2	0.00	0.00	0.05	0.00
Al_2O_3	33.38	33.27	32.35	33.70
FeO	6.67	7.20	6.08	6.46
MnO	0.26	0.19	0.52	0.68
MgO	8.41	8.23	8.74	7.98
CaO	0.00	0.00	0.09	0.04
Na_2O	0.64	0.42	0.38	0.25
K_2O	0.02	0.00	0.07	0.07
Total	97.81	97.03	95.18	97.82
Si	4.986	4.961	4.962	5.000
Ti	0.000	0.000	0.004	0.000
Al	4.047	4.074	4.030	4.081
Fe_2	0.574	0.626	0.538	0.556
Mg	1.291	1.276	1.378	1.223
Ca	0.000	0.000	0.010	0.004
Mn	0.023	0.017	0.047	0.059
Na	0.128	0.085	0.078	0.050
K	0.003	0.000	0.009	0.009
XMg	0.69	0.67	0.72	0.69

Note: G-Mig: Garnet-bearing migmatite; CGKfS-Mig: Cordierite-garnet-K-feldspar-sillimanite migmatite; inn-rim: inner rim; out-rim: outer rim; mid: middle point between core and rim; mtx: matrix.
XMg = Mg/(Mg + Fe). Abbreviations are the same for every part of Table 2.

assemblages. We estimated P-T conditions of ≈670 °C and 5.3 kbar on garnet cores (Table 3, Fig. 8a) combining calibrations from Holdaway (2000) for the Grt-Bt thermometer and the GBPQ barometer. P-T values for garnet rims combined with rim analysis of biotite and plagioclase in the matrix yielded temperatures of ≈615–640 °C (Holdaway, 2000) and pressures of ≈4.7–5.0 kbar (GBPQ, Wu et al., 2004).

Sample 7421 is a migmatite with leucosome assemblage Qtz + Pl + Grt ± Bt. Only mineral rims were analysed. Plagioclase is oligoclase composed by $Ab_{70}An_{27}Or_3$; biotite has X_{Mg} from 0.52 to 0.54 and Ti contents from 0.14 to 0.15 pfu (Table 2). Garnet is almandine with compositions $Alm_{63}Grs_3Prp_{19}Sps_{14}$. We calculated P-T conditions of ≈650–675 °C and 4.4–4.7 kbar on rim analysis by intersecting the GASP and Grt-Bt multivariant reactions. Combining Grt-Bt thermometry and GBPQ barometry we estimated P-T conditions of ≈655–670 °C and 4.8–5.1 kbar (Table 3, Fig. 8b).

5.3. Cordierite-garnet-K-feldspar-sillimanite migmatites

Leucosome of sample 7649 is characterized by a more biotite-rich domain and a cordierite-bearing leucocratic domain. In the biotite-rich domain plagioclase is andesine composed of $Ab_{63-67}An_{34-29}Or_{3-4}$, and biotite has X_{Mg} from 0.41 to 0.46 and Ti contents ranging from 0.17 to 0.20 pfu. Garnet is almandine with compositions $Alm_{62-63}Grs_{3-4}Prp_{13-20}Sps_{14-21}$ (Table 2). Garnet shows a slight compositional zoning with an increase in spessartine and a decrease in X_{Mg} towards the rim (Fig. 7c). In this domain, we estimated P-T conditions of ≈750–775 °C and 4.6–4.9 kbar on core analysis and of ≈650–705 °C and 3.3–3.7 kbar on rim analysis (Table 3, Fig. 8a) using the multiphase equilibria method (Berman, 1991). These results were tested by applying the conventional Grt-Bt thermometer and GBPQ geobarometer. Temperatures calculated applying conventional Grt-Bt thermometry (Holdaway, 2000) are

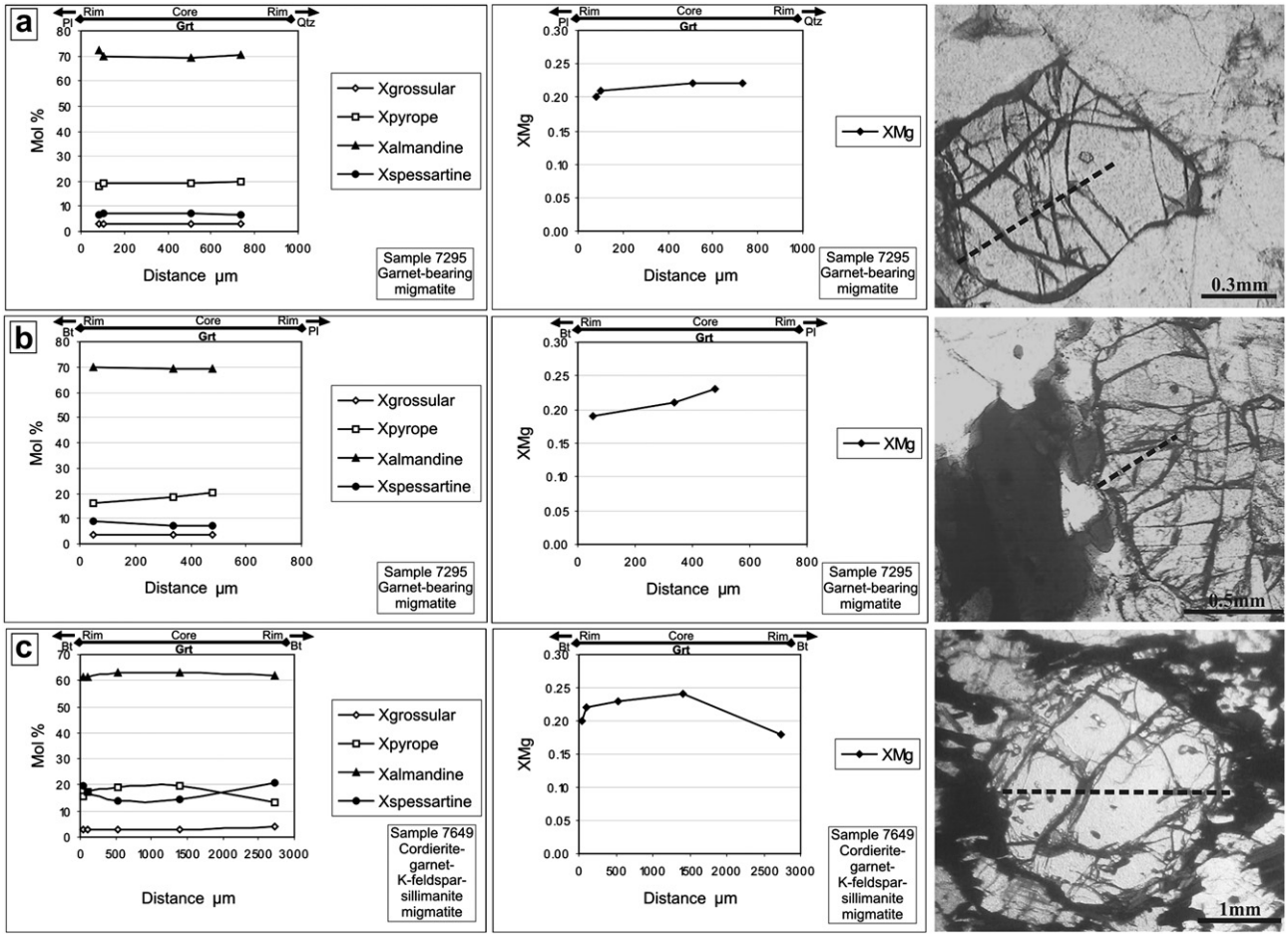

Fig. 7. Compositional garnet profiles. (a) and (b) Compositionally flat leucosome garnet of the garnet-bearing migmatites displaying typical profile of garnet that underwent diffusion processes at high grade conditions. Garnet in (b) was used in P-T calculations of sample 7295. (c) Garnet of the cordierite-garnet-K-feldspar-sillimanite migmatites showing slight compositional zoning with an increase in the spessartine component and a decrease in X_{Mg} towards the rim.

720–740 °C (core) and 660–700 °C (rim). GBPQ pressures range from 4.5 to 4.7 kbar (core) and from 3.8 to 4.0 kbar (rim). The cordierite-bearing domain lacks suitable assemblages for P-T calculations, a part of the Na-in-cordierite thermometry can be applied. In this domain, plagioclase is andesine composed of $Ab_{64-66}An_{31}Or_{3-5}$ and cordierite has X_{Mg} of 0.69–0.72 (Table 2). Biotite has X_{Mg} from 0.48 to 0.49 and Ti contents ranging from 0.16 to 0.17 pfu. A difference in Fe and Mg amounts is appreciable between biotite of both domains. Biotite within the biotite-rich domain where garnet is present has higher Fe contents and lower Mg contents than biotite within the cordierite-bearing domain (Fig. 9). On one hand, this could indicate compositional differences in the Mg/Fe ratio of the rock; on the other hand, this may reflect an increase in the Fe/Mg ratio of biotite caused by retrograde garnet resorption as observed in slightly reabsorved rims in some porphyroblasts. The occurrence of garnet-bearing mineral assemblages in the stability field calculated by the pseudosection is in acceptable agreement with the P-T conditions estimated by TWQ and conventional thermobarometry. By applying Na-in-cordierite thermometer on core analysis we calculated temperatures ranging from

Table 3
Summary of thermobarometric results.

Sample	Migmatite group	Mineral remarks	TWQ (multiphase equilibria)		Conventional thermobarometry		Na-in-Crd thermometry	
			T (°C)	P (kbar)	T (°C) Grt-Bt H00	P (kbar) GBPQ Wu04	T (°C) Wy07	T (°C) Mi08
7295	G-Mig	Core	670	5.2–5.3	670	5.3	–	–
		Rim	620–640	4.8–5.1	615–640	4.7–5.0	–	–
7421	G-Mig	Rim	650–675	4.4–4.7	655–670	4.8–5.1	–	–
7621	CGKfS-Mig	Core	–	–	–	–	730	715
		Mid	625	3.9	625	3.9	–	–
		Rim	615	3.6	615	3.7	635	585
7649	CGKfS-Mig	Core	750–775	4.6–4.9	720–740	4.5–4.7	740–800	735–820
		Rim	650–705	3.3–3.7	660–700	3.8–4.0	–	–

Note: G-Mig: Garnet-bearing migmatite; CGKfS-Mig: Cordierite-garnet-K-feldspar-sillimanite migmatite; mid: middle point between core and rim.
Calibrations: H00: Holdaway, 2000; Wu04: Wu et al., 2004; Wy07: Wyhlidal et al., 2007; Mi08: Mirwald et al., 2008.

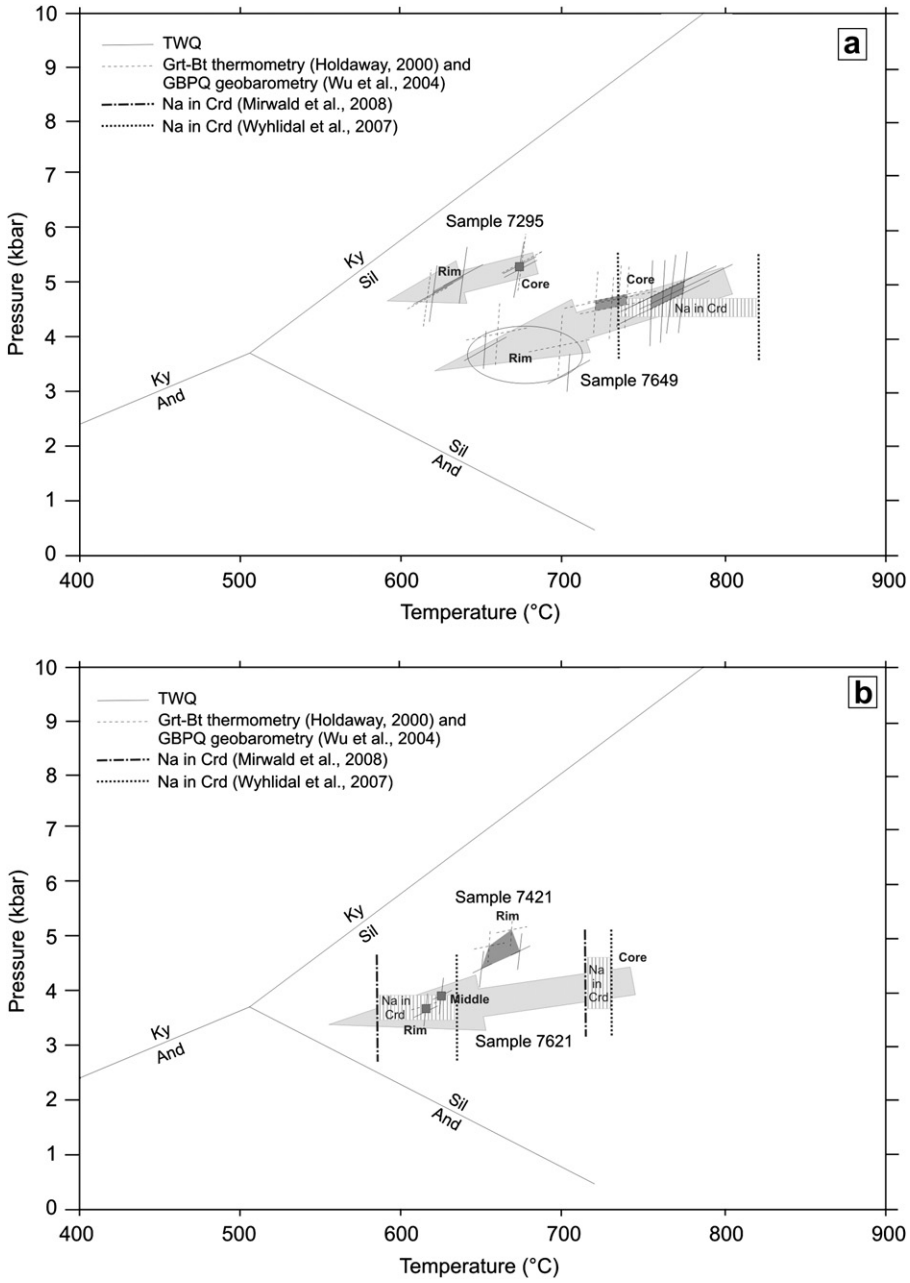

Fig. 8. P–T diagram showing peak metamorphic conditions derived from thermobarometry and deduced near isobaric cooling P-T trajectories from core to rim analysis. Aluminosilicate phase diagram from Holdaway (1971).

740 to 800 °C (calibration of Wyhlidal et al., 2007) and 735 to 820 °C (calibration of Mirwald et al., 2008) for the bearing-cordierite domain (Table 3). This roughly estimated temperature range is in satisfactory accordance, even a bit higher, with the stability field for the mineral assemblages Qtz + Pl + Kfs + Bt + Crd + Sil.

Sample 7621 is a migmatite with leucosome assemblage Qtz + Pl + Grt + Crd ± Bt. Plagioclase is oligoclase with compositions $Ab_{70-72}An_{29-27}Or_{1-2}$; biotite has Ti contents from 0.14 to 0.17 pfu and with X_{Mg} ranging from 0.52 to 0.54 except for a biotite included in garnet with X_{Mg} 0.58. Garnet is almandine with compositions $Alm_{69-71}Grs_3Prp_{17-18}Sps_{8-9}$ (Table 2) even though only middle and rim parts were analyzed. The middle section of garnet is slightly richer in the pyrope component and poorer in Fe and Mn than the garnet rim, with X_{Mg} ranging from 0.21 (middle part) to 0.19 (rim). P-T conditions of ≈625 °C and 3.9 kbar on garnet middle parts and of ≈615 °C and 3.6 kbar on garnet rims were calculated based on multiphase equilibria method (Table 3, Fig. 8b). Temperatures calculated applying conventional Grt-Bt thermometry were 625 °C (middle point) and 615 °C (rim). Pressures estimated based on GBPQ barometry were 3.9 kbar (middle point) and 3.7 kbar (rim). In this sample, one cordierite grain within the melanosome was analyzed. The cordierite has X_{Mg} of 0.67–0.69. Na-in-cordierite thermometry yielded temperatures of ≈730 °C (calibration of Wyhlidal et al., 2007) and 715 °C (calibration of Mirwald et al., 2008) on core analysis, and temperatures of ≈635 °C (calibration of Wyhlidal et al., 2007) and 585 °C (calibration of Mirwald et al., 2008) on rim analysis (Table 3). Cordierite rim temperatures are similar to those obtained for retrograde cooling

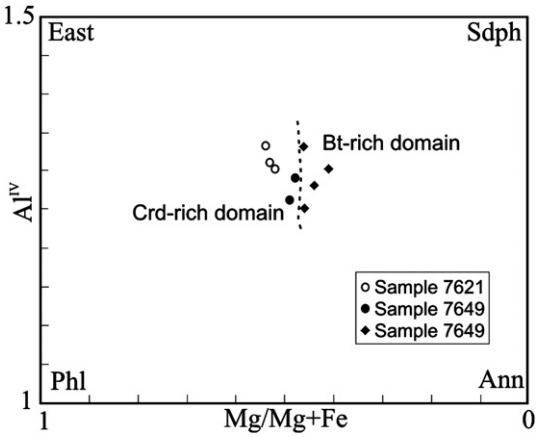

Fig. 9. Al^{IV} vs. Mg/Mg + Fe diagram displaying differences in Fe and Mg amounts between biotite from Crd-rich domains and Bt-rich domains in cordierite-garnet-K-feldspar-sillimanite migmatites.

temperatures on garnet rim. Cordierite core temperatures could indicate minimum estimates of near thermal peak conditions. However, the possibility of a re-equilibrium of cordierite during retrograde cooling is not excluded.

6. Geochronology

6.1. Previous geochronological data

In NW Argentina, Aceñolaza and Toselli (1976) proposed that the Famatinian Orogenic event was superposed on the Pampean Orogen. This hypothesis was recently confirmed in the Puna and northern Sierras Pampeanas by Lucassen and Becchio (2003), who dated the Pampean metamorphism at 530–510 Ma and the Famatinian superposed metamorphism at 470–420 Ma (U-Pb in titanite). Based on Rb-Sr dating (mineral/whole rock isochrons) two phases of metamorphism were distinguished in the Sierra de Ancasti and Sierra de Graciana: the first at 524 ± 28 Ma and the second at 472 ± 26 Ma (Knüver, 1983), the latter corresponding to the main metamorphism. Similar results were obtained by Bachmann and Grauert (1987a,b) from the Sierra de Ancasti with ages of 580–540 Ma and 470–435 Ma for the first and second metamorphic event respectively. In the nearby Sierra de Quilmes, Büttner et al. (2005) obtained a monazite U-Pb age of ≈470 Ma for the high grade metamorphism (migmatization) of the Sierra de Quilmes Metamorphic Complex.

6.2. U-Pb monazite geochronology

To constrain the timing of metamorphism, monazites from three different migmatite leucosomes from the EPMIC were dated (Fig. 1) using single grain U-Pb geochronology. In high-T metamorphic complexes, monazite U-Pb dating can be used to record ages that reflect the timing of peak conditions (or at least near) because this mineral has an adequate closure temperature (between 700 and 750 °C, Copeland et al., 1988; Hawkins et al., 1996; Rubatto et al., 2001) for the U-Pb isotopic system. Generally, it does not contain inherited cores and does not suffer radiogenic Pb loss at low temperatures (Parrish, 1990). The analyzed samples were 7444-leu from SE of the Sierra de Graciana (three monazite fractions), sample 7649-leu from N of the Sierra de Potrerillo (three monazite fractions), and sample 7550-leu from the central part of the Sierra de Potrerillo (two monazite fractions). The obtained results are presented in Table 4 and in Tera – Wasserburg Concordia diagrams

Table 4
U-Pb monazite data of the leucosome migmatites of El Portezuelo Metamorphic-igneous Complex.

SPU	Fraction	207/235[a]	Error	206/238[a]	Error	COEF.	238/206	Error	207/206[a]	Error	206/204[b]	Pb	U	Weight	206/238	207/235	207/206
Sample			(%)		(%)			(%)				(ppm)	(ppm)	mg	Age (Ma)	Age (Ma)	Age (Ma)
7444-leu																	
3840	A	0.58604	0.61	0.07597	0.47	0.791	13.16290	0.47	0.05595	0.38	180.19	658.1	3183.7	3.6	472	468	450
3841	B	0.59613	0.61	0.07579	0.58	0.942	13.19406	0.58	0.05705	0.21	638.98	476.0	2958.4	1.32	471	475	493
3842	C	0.59092	0.56	0.07578	0.48	0.859	13.19639	0.48	0.05656	0.29	2080.72	380.1	2309.8	5.42	471	471	474
7649-leu																	
3843	A	0.58632	0.51	0.07586	0.49	0.975	13.18150	0.49	0.05605	0.11	2183.48	332.0	1728.2	6.06	471	469	454
3844	B	0.58004	0.50	0.07485	0.49	0.974	13.36004	0.49	0.05620	0.11	8203.61	696.6	5067.4	4.25	465	464	460
3845	C	0.59532	0.64	0.07652	0.61	0.959	13.06875	0.61	0.05643	0.18	1913.77	447.0	2271.0	5.08	475	474	469
7550-leu																	
3846	A	0.62194	2.34	0.07690	1.61	0.691	13.00350	1.61	0.05866	1.69	308.53	252.1	1022.5	1.51	478	491	554
3847	B	0.58856	1.50	0.07662	1.43	0.960	13.05122	1.43	0.05571	0.42	180.79	168.0	621.1	1.51	476	470	441

Note: SPU: laboratory number. Fractions: numbers in parentheses indicated the number of grains handpicked.
Ages: given in Ma using Ludwig Isoplot/Ex program (1998), decay constants recommended by Steiger and Jäeger (1977).
[a] Radiogenic Pb corrected for blank and initial Pb. U corrected for blank.
[b] Not corrected for blank or non-radiogenic Pb. Total U and Pb concentrations corrected for analytical blank.

(Fig. 10). Monazite analysis yield mean $^{206}Pb/^{238}U$ ages of 471 ± 1 Ma for sample 7444-leu, 470 ± 12 Ma for sample 7649-leu, and 477 ± 5 Ma for sample 7550-leu. The age of 471 ± 1 Ma obtained from sample 7444-leu is interpreted as the most precise age of the migmatization. We can constrain the crystallization of the anatectic melts to the Lower - Middle Ordovician.

7. Discussion

7.1. Metamorphic evolution, P-T conditions and age of migmatites

The petrographic study combined with thermobarometric data allows qualitative and quantitative characterization of the peak metamorphic conditions and metamorphic evolution of migmatites of the EPMIC. Although the reaction textures and mineral rim-core compositions (and hence the P-T paths) in poly-phase metamorphic terrains could be related to two o more phases widely separated in time (e.g. Vernon, 1996), our well constrained geochrological data indicate that the migmatization event occurred during a single metamorphic episode. The first approach on the basis of petrography and field studies suggests that the metasedimentary unit (EPMIC) underwent high grade metamorphic conditions (and anatexis) and all migmatites were developed above the second sillimanite isograd, as evidenced by: 1- the total absence of muscovite as primary phase, 2- presence of partial melting represented by leucosomes and diatexites; 3- existence of mineral assemblages indicative of melt-forming reactions; and 4- the occurrence of microstructures and macrostructures associated with melting (e.g. crystal faces of plagioclase, interlobate association of garnet and quartz, schlieren, rafts of resisters, igneous-like texture). A short prograde metamorphic evolution can be deduced within migmatite blocks. The garnet-absent migmatites with Qtz + Pl + Bt + Kfs + Sil mineral assemblage would represent relatively lower metamorphic grade rocks, whereas the cordierite-garnet-K-feldspar-sillimanite migmatites represent higher metamorphic grade rocks. Thus, the migmatite metamorphic evolution took place from amphibolite to granulite facies conditions at similar pressures. Consistently, this assumption is supported by pseudosections where gradual mineral changes are evident during the metamorphic prograde evolution of melted rocks from Qtz + Pl + Bt + Kfs + Sil + melt stability field to Qtz + Pl + Bt + Kfs ± Sil ± Grt ± Crd + melt stability fields (Fig. 6). These changes are restricted within a tight range of temperatures from ≈670 °C where melting started at ≈750 °C where cordierite and garnet coexisting appear. The range of temperatures estimated according to minimum partial melting conditions of metasedimentary rocks ($T > 630$ °C and $P > 4$ kbar, Sawyer, 1999; ≈650 °C, Vernon, 2004). Supporting this argument, calculated temperatures and pressures based on conventional thermobarometry agree with petrographic observations and pseudosections thermobarometry. Maximum metamorphic P-T conditions are ≈ 750–775 °C and 4.6–4.9 kbar, and were calculated for the cordierite-garnet-K-feldspar-sillimanite migmatites. Therefore these P-T conditions should be considered as the closest estimate of thermal peak conditions. Additionally, Na-in-cordierite thermometry suggests that the cordierite-garnet-K-feldspar-sillimanite migmatites underwent a slightly higher temperature of around 800–820 °C. Slightly higher pressures may have been reached as predicted by pseudosections and pressures calculated in garnet-bearing cordierite-free domains and in the garnet-bearing migmatites. In any case, the migmatites of the EPMIC did not undergo pressures higher than ≈5.5 kbar. Lower T peak conditions of ≈670 °C were estimated in garnet-bearing migmatites (sample 7295). Probably temperatures were higher since cores of the small-sized garnets analyzed (diameters < 1 mm) may have been affected by diffusion during cooling. The P-T conditions estimated in the EPMIC are consistent with high T/P metamorphism developed at about 17–21 km depth (assuming an average density of 2800 kg/m^3). Since the middle crust is generally dominated by rocks metamorphosed at amphibolite facies to lower granulite

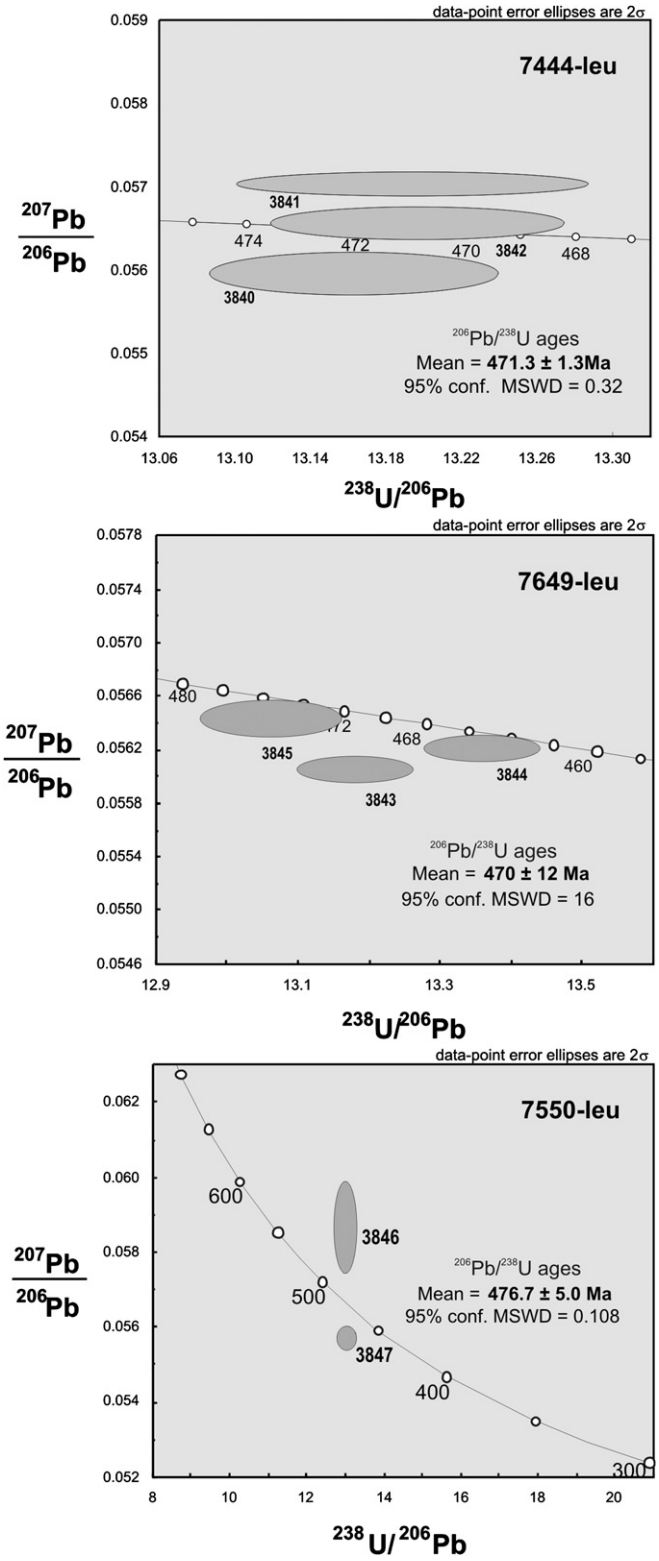

Fig. 10. U-Pb monazite isotopic analyses plotted in Tera-Wasserburg diagrams. Data-point error ellipses are 2σ. Mean $^{206}Pb/^{238}U$ ages are indicated in bold.

facies (Rudnick and Gao, 2003; and references therein) the current exposed paleo-depths and anatectic rocks of the EPMIC are representative of Early Ordovician mid-crustal levels.

The ages obtained from monazites in leucosomes of migmatites provide a good constraint on the timing of the high T/P metamorphism in the EPMIC. The anatectic event took place during the lower to medium Ordovician boundary, in a time restricted to ≈477–470 Ma. This age agrees with less reliable Rb-Sr age estimations of 472 ± 26 Ma determinated by Knüver (1983) for high grade rocks of the nearby Sierra de Ancasti generated during a low-medium regional metamorphism pressure (Willner, 1983). The accurate monazite U-Pb dating of the migmatization event rules out the idea that the main metamorphic event occurred during the Pampean orogeny. Taking into account that migmatite terranes are widely distributed in several neighbouring basement blocks (Sierra de Ancasti, Sierra de Ambato, Sierra de Aconquija), and that they can be directly related to the EPMIC, the metamorphic conditions and the previously established ages imply the existence of a regional mid-crustal high thermal zone during lower-medium Ordovician times.

7.2. P-T paths and tectonic setting

The retrograde P-T paths of migmatites were deduced by using core-rim thermobarometric data. The P-T trajectories in garnet-bearing migmatites and cordierite-garnet-K-feldspar-sillimanite migmatites are characterized by P/T gradients ranges of 0.3–1.2 kbar/100 °C and 0.5–1.5 kbar/100 °C respectively, indicating near isobaric cooling paths (Fig. 8). The petrologic interpretations on these deduced paths should be carefully considered, due to possible effects of variable closure temperature for geothermometers and geobarometers and the amount of mineral phases that reacted during cooling (e.g. Frost and Chacko, 1989; Harley, 1989). Isobaric cooling paths are more difficult to interpret unless some portion of prograde P-T path can be deduced (Spear, 1993). Since prograde evolution was not resolved for the EPMIC, the retrograde part of an isobaric cooling path could be related to an elevated geotherm caused by heat sources beneath the crust (the magma underplating model; Ellis, 1987). The lack of relic mineral assemblages linked to a hypothetical previous high pressure prograde metamorphism support the idea of the magma underplating model. Furthermore, textures indicating isothermal decompression (Harley, 1989; Brown, 2002) such as corona structures produced by the reaction Grt + Sil + Qtz = Crd were not observed. The widespread Ordovician magmatism coeval with mid-crustal high T/P metamorphism in the Famatinian belt (Pankhurst et al., 2000; Lucassen and Franz, 2005) supports the idea of high heat flux linked to thermal regimes. The mineralogical and textural evidence, the peak metamorphic conditions estimated and the near isobaric cooling P-T paths deduced in migmatites of the EPMIC suggest a non colisional setting, rather associated to high isostatical stability of the Famatinian middle crust during a high thermal regime. Isobaric cooling paths rule out significant decompression after the thermal peak metamorphism. This is consistent with Paleozoic moderate and slow rates of exhumation estimated by de los Hoyos et al. (submitted for publication) in the eastern Sierra de Velasco. It is possible that slow exhumation led to long residence of the middle crust under high temperature at similar crustal level during the Ordovician, as suggested by wide-ranging metamorphic and cooling ages in the Famatinian basement (Lucassen and Becchio, 2003; Büttner et al., 2005).

7.3. Regional implications for the Famatinian orogen

Similar high temperature relatively low-medium pressure metamorphic conditions, retrograde isobaric cooling paths and ages could be related along ≈1000 km (26°–33°S) and ≈250 km (65°–68°W) throughout the Famatinian belt. From north to south this high thermal regime, characterized by high grade metamorphism and associated coeval magmatism, has been recognized in Quilmes (Rossi de Toselli et al., 1987; Büttner et al., 2005), Ancasti, Ambato and Aconquija (this work); Velasco (de los Hoyos et al., submitted for publication), Chepes (Dahlquist and Baldo, 1996); Valle Fértil – La Huerta (Otamendi et al., 2008) and San Luis (Hauzenberger et al., 2001; Delpino et al., 2007) ranges. At about 31°–32° southern latitude, a geological setting for the Famatinian belt has been proposed by Otamendi et al. (2008) based on peak metamorphic P-T conditions and trajectories deduced of several

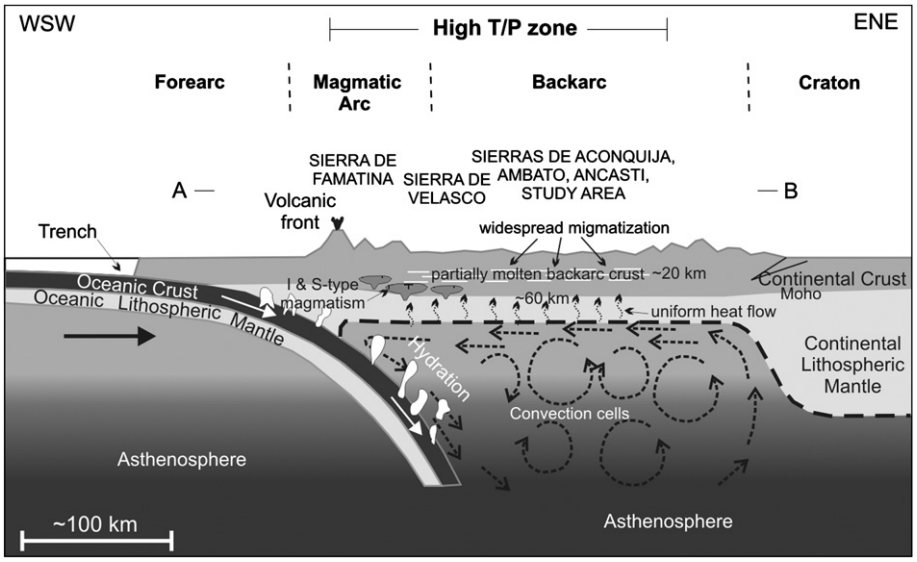

Fig. 11. Thermal-tectonic conceptual model across the Famatinian belt (adapted from and modified after Hyndman et al., 2005) showing uniform heat-flow operating over a wide high T/P back-arc mid-crustal segment as consequence of shallow convection of a low-viscosity asthenosphere promoted by subducting-slab dehydration. A–B indicates the direction of the cross section drew in Fig. 1.

localities integrated across a latitudinal transect. In this geodynamic setting Otamendi et al. (2008) defined from east to west: 1- a back-arc zone represented for the Pringles Complex in the Sierra de San Luis with metamorphic evolution characterized by heating-cooling paths at ≈5.7 kbar of pressure (Hauzenberger et al., 2001; Delpino et al., 2007); 2- an arc zone showing different crustal levels: a- an upper arc crust defined in the Sierra de Chepes with low-P metamorphic conditions ($P < 3$ kbar) within the main axis of Famatinian arc (Dahlquist and Baldo, 1996), and b- a lower arc crust represented by granulite-facies migmatites showing heating-cooling trajectories at 5–7 kbar of pressure in the Sierras de Valle Fértil-La Huerta; 3- an accretionary wedge in the west side of the Sierra de Valle Fértil (Las Chacras region) interpreted the most deeply exhumed section of the Famatinian crust evidenced by relatively strong isothermal decompression paths (Vujovich, 1994; Baldo et al., 2001). Therefore, and considering recent metamorphic conditions and deduced P-T paths (Büttner et al., 2005; de los Hoyos et al., submitted for publication; this work), the regional contact metamorphism for the back-arc and main arc axis of the Famatinian belt between 31° and 33° south latitude proposed by Otamendi et al. (2008) could be spread out to the north until 26° S. In this regional context the high grade metamorphic basement with minor magmatic activity (Quilmes, Ancasti, Ambato, Aconquija ranges, and the study area) corresponds to the back-arc environment, whereas the westward zone characterized by abundant Ordovician magmatism (Sierra de Capillitas, Sierra de Velasco) would represent the lower levels in the main axis of the Famatinian arc (Fig. 1). The ages obtained in the study area (470–477 Ma) allow us to relate the high T/P migmatization event with those developed in the Sierra de Quilmes (470 Ma; Büttner et al., 2005) and Sierra de San Luis (478 Ma; Steenken et al., 2006) in agreement with the assumption of a back-arc anatectic area developed along the eastern part of Famatinian belt from 26° to 33°S.

7.4. Probable mechanism for uniform heating of the Famatinian back-arc

Widespread migmatization and magmatism in the Famatinian crust requires rather uniform heat input over a great crustal area. High lithosphere temperatures across back-arcs are a common feature of several current orogenic belts (Hyndman et al., 2005). We propose a geodynamic setting based on the classic model of a mobile belt generated during continentward subduction of an oceanic slab beneath continental margin (Hyndman and Lewis, 1999). The migmatites of the study area and nearby regions represent a heated and thermally-weakened back-arc middle crust. Uniform high rates of heat-flow operating over a wide mid-crustal segment (Fig. 11) can be explained by strong and fast regional small-scale convection cells beneath the continental crust (Currie et al., 2004). In this model, shallow asthenosphere convection is aided by water generated from dehydration of the underlying subducted slab, which causes viscosity decrease in the overlying asthenospheric wedge (Hyndman et al., 2005; and references therein). Since dehydration of a subducted oceanic slab occurs at ≈60–105 km depth (Arcay et al., 2005), a relatively shallow-dipping slab is required to cause the continentward wide zone of partial melting of the Famatinian middle crust. This supports the previous hypothesis by Willner et al. (1987) of shallow-dipping subduction during the Lower Paleozoic geodynamic evolution of the Famatinian belt at 29°S.

8. Conclusions

Petrologic, thermobarometric and geochronologic data presented in this work allow postulation of the following conclusions:

1. The migmatites of the El Portezuelo Metamorphic-Igneous Complex evolved above the second sillimanite isograd from amphibolite to granulite facies conditions. The thermal peak metamorphic conditions were 670–820 °C and 4.5–5.3 kbar consistent with a high T/P metamorphism developed at about 17–21 km depth, representative of mid-crustal levels.
2. The anatectic event took place during the lower to medium Ordovician boundary, in a time restricted to between 477 and 470 Ma. The metamorphic conditions and the ages here presented imply the existence of a wide high thermal mid-crustal zone during Lower - Medium Ordovician times in the northern Sierras Pampeanas.
3. Regional Ordovician post-peak isobaric cooling suggests slow and homogeneous exhumation and longstanding high-thermal residence for the middle crust of the Famatinian back-arc.
4. Shallow convection of a low-viscosity asthenosphere, promoted by subducting-slab dehydration (Hyndman et al., 2005) could explain the widely distributed uniform high thermal back-arc gradients in a wide mid-crustal segment of the Famatinian belt.

Acknowledgements

This work was funded by CONICET Grant no. PICT 0159, ANPCyT PICT Grant no. 07-09686, and CIUNT Grant no. 26-G222. ANPCyT and CONICET are thanked for scholarships awarded to M. Larrovere during his PhD studies. We thank J. Palavecino for his help with field work. We specially acknowledge J. de la Rosa for providing a whole-rock chemical analysis. We are grateful to P. Alasino, E. Baldo and S. Verdecchia for their comments. Technical support from INSUGEO-CONICET, Universidad Nacional de Tucumán, CRILAR-CONICET, CPGeo-Universidade de São Paulo, and Universidad de Chile in the preparation of this work is acknowledged. We are grateful to J. Otamendi and A. Steenken for their thoughtful and constructive reviews that greatly improved the quality of this article.

Appendix

Geothermobarometry

The mineral chemical analyses were carried out at the electronic microscopy laboratory of the Geology Department of the Universidad de Chile using a SEM-Probe CAMEBAX SU-30. All elements were measured using Wavelength Dispersive X-ray Spectroscopy (WDS). Quantitative analysis using software XMAS 7.0, with ZAF correction, the beam current was 10 nA, the accelerating voltage was 15 kV, counting times of 10 s, and the beam diameter was 2 μm (mode fix). Silicates and oxides standards certified by P&H Developments were used. The quality of mineral chemical data was evaluated on the basis of stoichiometry of the minerals. A deviation of 2% from stoichiometry was generally accepted as an upper limit. Exceptions were made for biotite due to the inevitable effect of Na and K loss during measurements and imperfect stoichiometry of natural biotites. The elements measured were Si, Al, Ti, Fe, Mg, Mn, Na, Ca, and K. Mineral structural formulas were calculated using CalcMin and Minpet software.

Whole-rock major elements geochemistry used in pseudosecions was determined at the Universidad de Oviedo, Spain, by X-ray fluorescence (XRF) with a Phillips PW2404 system using glass beads, and at Activation Laboratories, Ontario, Canada, by ICP following the procedure 4-Lithoresearch code.

U-Pb geochronology

U-Pb geochronology was carried out at the Centro de Pesquisas Geocronológicas of the Universidade de São Paulo, Brazil. The isotopic dilution method ID-TIMS (Isotope Dilution – Thermal Ionization Mass Spectrometry) was applied. Monazite concentrates were obtained using standard crushing and sieved, and separated using a vibrating table, magnetic separation and heavy liquids treatment (for details see Passarelli et al., 2009). Complete, translucent, clear and crack-free monazite crystals were handpicked under alcohol from this concentrate using a stereoscope that is coupled with an imaging system. The monazite crystals were washed with 6N HCL, 7N HNO_3 and H_2O (MiliQ). The material was further stored in 14N HNO_3. Chemical digestion took place in 3 ml screw-top PFA Savillex vials, with the addition of one micro-drop of HNO_3 and 7 μl of ultra pure H_2SO_4. Also the tracer 205 (10 μl) is added in the Savillex. The vials stood on a hot plate for three days. After chemical digestion, the solution was transferred to a 7 ml savillex and dry-evaporated. Next, 6N HCL was added and the savillex stood on a hot place overnight. Subsequently the solution was dry-evaporated and dissolved in 3N HCL. The U and Pb of the samples were separated using an anion exchange columns with Eichrom resin 1 × 8200 of 400 mesh. Pb and U were loaded on Re filaments. The isotopic ratios of Pb and U were determined with a multicollector Finnigan MAT 262 mass spectrometer. The results were treated by ISOPLOT (Ludwig, 1998) software. The constants used in the age calculations are from Steiger and Jäeger (1977). All errors used are at the 95% (2σ) confidence level.

References

Aceñolaza, F.G., Toselli, A.J., 1976. Consideraciones estratigráficas y tectónicas sobre el paleozoico inferior del noroeste argentino. 2° Congreso Latinoamericano de Geología, 755–763, Caracas, (1973).

Aceñolaza, F.G., Toselli, A.J., 1977. Esquema Geológico de la Sierra de Ancasti, provincia de Catamarca. Acta Geológica Lilloana 14, 233–256.

Aceñolaza, F.G., Toselli, A.J., 1981. Geología del Noroeste Argentino. Universidad Nacional de Tucumán, Tucumán, 212 pp.

Aceñolaza, F.G., Miller, H., 1982. Early Palaeozoic orogeny in southern south America. Precambrian Research 17, 133–146.

Aceñolaza, F.G., Durand, F.R., 1986. Upper Precambrian – Lower Cambrian biota from the northwest of argentina. Geological Magazine 123, 367–375.

Aceñolaza, F.G., Miller, H., Toselli, A.J., 2000. The Pampean and Famatinian Cycles-superposed orogenic events in west Gondwana. Zeitschrift für Angewandte Geologie 1, 337–344. Sonderheft SH.

Adams, C.J., Miller, H., Toselli, A.J., 1990. Nuevas edades de metamorfismo por el método K-Ar de la Formación Puncoviscana y equivalentes, NW de argentina. In: Aceñolaza, F.G., Miller, H., Toselli, A.J. (Eds.), El Ciclo Pampeano en el noroeste Argentino. Serie Correlación Geológica 4. Universidad Nacional de Tucumán, San Miguel de Tucumán, pp. 209–219.

Arcay, D., Tric, E., Doin, M.P., 2005. Numerical simulations of subduction zones. Effect of slab dehydration on the mantle wedge dynamics. Physics of the Earth and Planetary Interiors 149, 133–153.

Bachmann, G., Grauert, B., 1987a. Datación de metamorfismo basado en el análisis isotópico Rb/Sr en perfiles de pequeña sección de metasedimentos polimetamórficos en el Noroeste Argentino. In: 10° Congreso Geológico Argentino III, 17–20.

Bachmann, G., Grauert, B., 1987b. Análisis isotópico Rb/Sr y edad del granate - almandino en los gneises bandeados polimetamórficos de la Sierra de Ancasti y Tafí del Valle (Sierras Pampeanas, NW – Argentina). In: 10° Congreso Geológico Argentino, III, 21–24.

Baldo, E., Casquet, C., Rapela, C.W., Pankhurst, R., Galindo, C., Fanning, C., Saavedra, J., 2001. Ordovician metamorphism at the southwestern margin of Gondwana: P-T conditions and U-Pb SHRIMP ages from Loma de Las Chacras, Sierras Pampeanas. In: III Simposio Sudamericano de Geología Isotópica 3, 544–547.

Berman, R.G., 1991. Thermobarometry using multiequilibrium calculations: a new technique, with petrological applications. Canadian Mineralogist 29, 833–855.

Berman, R.G., Aranovich, L.Y.A., 1996. Optimized standard state and solution properties of minerals: I. Model calibration for olivine, orthopyroxene, cordierite, garnet, and ilmenite in the system FeO–MgO–CaO–Al_2O_3–TiO_2–SiO_2. Contributions to Mineralogy and Petrology 126, 1–24.

Berman, R.G., Aranovich, L.Ya., Rancourt, D.G., Mercier, P.H.J., 2007. Reversed phase equilibrium constraints on the stability of Mg-Fe-Al biotite. American Mineralogist 92 (1), 139–150.

Brown, M., 2001. Orogeny, migmatites and leucogranites: a review. Journal of Earth System Science 110 (4), 313–336.

Brown, M., 2002. Retrograde processes in migmatites and granulites revisited. Journal of Metamorphic Geology 2, 25–40.

Büttner, S.H., Glodny, J., Lucassen, F., Wemmer, K., Erdmann, S., Handler, R., Franz, G., 2005. Ordovician metamorphism and plutonism in the Sierra de Quilmes metamorphic complex: implications for the tectonic setting of the Northern Sierras Pampeanas (NW Argentina). Lithos 83, 143–181.

Caminos, R., 1979. Sierras Pampeanas Noroccidentales. Salta, Tucumán, Catamarca, La Rioja y San Juan. In: 2° Simposio de Geología Regional Argentina, vol. I 225–291.

Connolly, J.A.D., 1990. Multivariable phase diagrams; an algorithm based on generalized thermodynamics. American Journal of Sciences 290, 666–718.

Copeland, P., Parrish, R.R., Harrison, T.M., 1988. Identification of inherited radiogenic Pb in monazite and its implications for U-Pb systematic. Nature 333, 760–763.

Currie, C.A., Wang, K., Hyndman, R.D., He, J., 2004. The thermal effects of slab-driven mantle flow above a subducting plate: the Cascadia subduction zone and back-arc. Earth and Planetary Earth Science Letters 223, 35–48.

Dahlquist, J.A., Baldo, E.G., 1996. Metamorfismo y deformación famatinianos en la Sierra de Chepes, La Rioja, Argentina. In: XIII Congreso Geológico Argentino y III Congreso de Exploración de Hidrocarburos 5, 393–409.

de los Hoyos, C.R., Willner, A.P., Larrovere, M.A., Rossi, J.N., Toselli, A.J., Basei, M.A.S., 2010. Tectonothermal evolution and exhumation history of the Paleozoic Proto-Andean Gondwana margin crust: The Famatinian Belt in NW Argentina. Gondwana Research. doi:10.1016/j.gr.2010.12.004.

Delpino, S.H., Bjerg, E.A., Ferracutti, G.R., Morgessie, A., 2007. Counterclockwise tectonometamorphic evolution of the Pringles metamorphic complex, Sierras Pampeanas of San Luis (Argentina). Journal of South American Earth Sciences 23, 147–175.

Ellis, D.J., 1987. Origin and evolution of granulites in normal and thickened crusts. Geology 15, 167–170.

Frost, B.R., Chacko, T., 1989. The granulite uncertainty principle: limitations on thermobarometry in granulites. Journal of Geology 97, 435–450.

Fuhrman, M.L., Lindsley, D.H., 1988. Ternary-feldspar modelling and thermometry. American Mineralogist 73, 201–216.

Ghent, E.D., Grover, T.W., 1995. Calculation of the activity of Al_2SiO_5: applications to the geobarometry and geohygrometry of garnet and staurolite zone metapelitic rocks. American Journal of Science 295, 923–942.

Grosse, P., Söllner, F., Báez, M.A., Toselli, A.J., Rossi, J.N., de la Rosa, J.D., 2009. Lower Carboniferous post-orogenic granites in central-eastern Sierra de Velasco, Sierras Pampeanas, Argentina: U-Pb monazite geochronology, geochemistry and Sr-Nd isotopes. International Journal Earth Sciences 98, 1001–1025.

Harley, S.L., 1989. The origin of granulites: a metamorphic perspective. Geological Magazine 126, 215–247.

Hauzenberger, C.A., Morgessie, A., Hoinkes, G., Felfernig, A., Bjerg, E.A., Kostadinoff, J., Delpino, S., Dimieri, L., 2001. Metamorphic evolution of the Sierra de San Luis: granulite facies metamorphism related to mafic intrusions. Mineralogy and Petrology 71 (1/2), 95–126.

Hawkins, D.P., Bowring, S.A., Ilg, B.R., Kalstrom, K.E., Wiliams, M.L., 1996. U-Pb geochronologic constraints on the Paleoproterozoic crustal evolution of the upper granite Gorge, Grand Canyon, Arizona. Geological Society of American Bulletin 108, 1167–1181.

Höckenreiner, M., Söllner, F., Miller, H., 2003. Dating the TIPA shear zone: an Early Devonian terrane boundary between Famatinian and Pampean systems (NW Argentina). Journal of South American Earth Sciences 16, 45–66.

Holdaway, M.J., 1971. Stability of andalusite and the aluminium silicate phase diagram. American Journal of Sciences 271, 97–131.

Holdaway, M.J., 2000. Application of new experimental and garnet Margules data to the garnet-biotite geothermometer. American Mineralogist 85, 881–892.

Holland, T.J.B., Powell, R., 1998. An internally consistent thermodynamic data set for phases of petrological interest. Journal of Metamorphic Geology 16, 309–343.

Huang, W.L., Wyllie, P.J., 1974. Melting relations of muscovite with quartz and sanidine in the K_2O–Al_2O_3–SiO_2–H_2O system to 30 kilobars and an outline of paragonite melting relations. American Journal of Sciences 274, 378–395.

Hyndman, R.D., Lewis, T.S., 1999. Geophysical consequences of the Cordillera-Craton thermal transition in S.W. Canada. Tectonophysics 306, 397–422.

Hyndman, R.D., Currie, C.A., Mazzotti, S.P., 2005. Subduction zone backarcs, mobile belts, and orogenic heat. GSA Today 15 (2), 4–10.

Indri, D.A., Barber, L.E., 1987. Características geológicas y químicas del granito San Ignacio - Los Pinos, Provincias de Tucumán y Catamarca, Argentina. In: 10° Congreso Geológico Argentino, IV, 135–138.

Jordan, T., Allmendinger, R., 1986. The Sierras Pampeanas of Argentina: a modern analogue of Rocky mountain foreland deformation. American Journal of Science 286, 737–764.

Knüver, M., 1983. Dataciones radimétricas de rocas plutónicas y metamórficas. In: Aceñolaza, F.G., Miller, H., Toselli, A.J. (Eds.), La Geología de la Sierra de Ancasti, vol. 59. Münstersche Forschungen zur Geologie und Paläontologie, Münster, pp. 201–218.

Kraemer, P.E., Escayola, M.P., Martino, R.D., 1995. Hipótesis sobre la evolución tectónica neoproterozoica de las Sierras Pampeanas de Córdoba (30°40'–32°40'S), Argentina. Revista de la Asociación Geológica Argentina 50, 47–59.

Larrovere, M.A., Toselli, A.J., Rossi de Toselli, J.N., 2008. Petrología y estructura de la Faja de Deformación La Chilca, Catamarca, Argentina. Revista de la Asociación Geológica Argentina 63 (2), 94–103.

Larrovere, M. Petrología de la faja migmatítica entre el flanco noroccidental de la Sierra de Ancasti, su continuación en la Sierra de Aconquija y el flanco

nororiental de la Sierra de Ambato. Doctoral thesis, Universidad Nacional de Córdoba (unpublished), 234 p.
Le Corre, C.A., Rossello, E.A., 1994. Kinematics of early Paleozoic ductile deformation in the basement of NW Argentina. Journal of South American Earth Sciences 7, 301–308.
López, J.P., Sales de López, A., Stipp Basei, M., 2000. Nueva edad K/Ar en la historia deformativa de la Faja Milonítica Tipa, en el Noroeste Argentino. Zentralblatt für Geologie und Paläontologie I (7/8), 895–902.
Lork, A., Miller, H., Kramm, U., Grauert, B., 1990. Sistemática U-Pb de circones detríticos de la Formación Puncoviscana y su significado para la edad máxima de sedimentación en la Sierra de Cachi (Provincia de Salta, Argentina). In: Aceñolaza, F.G., Miller, H., Toselli, A.J. (Eds.), El Ciclo Pampeano en el noroeste Argentino. Serie Correlación Geológica, vol. 4. Universidad Nacional de Tucumán, San Miguel de Tucumán, pp. 199–208.
Lucassen, F., Becchio, R., Wilke, H.G., Franz, G., Thirlwall, M.F., Viramonte, J., Wemmer, K., 2000. Proterozoic – Paleozoic development of the basement of the Central Andes (18–26°) - a mobile belt of the South American craton. Journal of South American Earth Science 13, 697–715.
Lucassen, F., Becchio, R., 2003. Timing of high-grade metamorphism: early Palaeozoic U-Pb formation ages of titanite indicate long-standing high-T conditions at the western margin of Gondwana (Argentina, 26–29°S). Journal of Metamorphic Geology 21, 649–662.
Lucassen, F., Franz, G., 2005. The early paleozoic orogen in the central Andes: a non-collisional orogen comparable to the cenozoic high plateau? In: Vaughan, A.P.M., Leat, P.T., Pankhurst, R.J. (Eds.), Terrane Processes at the Margins of Gondwana Geological Society of London, Special Publications, 246, pp. 257–373.
Ludwig, K.R., 1998. Using Isoplot/Ex. A Geochronological Toolkit for Microsoft Excel. Berkeley Geochronology Center. Special Publication No 1.
Miller, H., Willner, A., 1981. The Sierra de Ancasti (Catamarca Province), an example of polyphase deformation of Lower Paleozoic age in the Pampean Ranges. Zentralblatt für Geologie und Paläontologie I (3/4), 272–284.
Millord, I., Sawyer, E.W., 2003. Schlieren formation in diatexite migmatite: examples from the St Malo migmatite terrane, France. Journal of Metamorphic Geology 21, 347–362.
Mirwald, P.W., Scola, M., Tropper, P., 2008. Experimental study on the incorporation of Na in Mg-cordierite in the presence of different fluids (Na (OH), NaCl–H_2O, albite-H_2O). Geophysical Research Abstracts 10 SRef-ID: 1607–7962/gra/EGU2008-A-04149.
Otamendi, J.E., Patiño Douce, A.E., Demichelis, A.H., 1999. Amphibolite to granulite transition in aluminous greywackes from the Sierra de Comechingones, Córdoba, Argentina. Journal of Metamorphic Geology 17, 415–434.
Otamendi, J.E., Tibaldi, A.M., Vujovich, G.I., Viñao, G.A., 2008. Metamorphic evolution of migmatites from the deep Famatinian arc crust exposed in Sierras Valle Fértil-La Huerta, San Juan, Argentina. Journal of South American Earth Sciences 25, 313–335.
Pankhurst, R.J., Rapela, C.W., Fanning, C.M., 2000. Age and origin of coeval TTG, I- and S-type granites in the Famatinian belt of NW Argentina. Transactions of the Royal Society of Edinburgh: Earth Sciences 91, 151–168.
Parrish, R.R., 1990. U-Pb dating of monazite and its application to geological problems. Canadian Journal of Earth Sciences 27, 1431–1450.
Passarelli, C.R., Basei, M.A.S., Siga Jr., O., Sato, K., Sproesser, W.M., Loios, V.A.P., 2009. Dating minerals by ID-TIMS geochronology at times of *in situ* analysis: selected case studies from the CPGeo-IGc-USP laboratory. Anais da Academia Brasileira de Ciencias 81 (1), 73–97.
Patiño Douce, A.E., Johnston, A.D., Rice, J.M., 1993. Octahedral excess mixing properties in biotite: a working model with applications to geobarometry and geothermometry. American Mineralogist 78, 113–131.
Ramos, V.A., Jordan, T.E., Allmendinger, R.W., Mpodozis, C., Kay, S.M., Cortés, J.M., Palma, M., 1986. Paleozoic terranes of the central Argentine Chilean Andes. Tectonics 5, 855–880.
Ramos, V.A., 1988. Late Proterozoic - Early paleozoic of south America: a collisional history. Episodes 11, 168–174.
Ramos, V.A., Cristallini, E.O., Pérez, D.J., 2002. The Pampean flat-slab of the central Andes. Journal of South American Earth Sciences 15, 59–78.
Ramos, V.A., Vujovich, G., Martino, R., Otamendi, J., 2010. Pampia: a large cratonic block missing in the Rodinia supercontinent. Journal of Geodynamics 50, 243–255.
Rapela, C.W., Pankhurst, R.J., Casquet, C., Baldo, E., Saavedra, J., Galindo, C., Fanning, C.M., 1998. The Pampean orogeny of the southern proto-Andes: evidence for Cambrian continental collision in the Sierras de Córdoba. In: Pankhurst, R.J., Rapela, C.W. (Eds.), The Proto-Andean Margin of Gondwana. Geological Society of London, Special Publication, 142, pp. 181–217.
Rapela, C.W., Casquet, C., Baldo, E., Dahlquist, J., Pankhurst, R.J., Galindo, C., Saavedra, J., 2001. Las Orogénesis del Paleozoico Inferior en el margen proto-andino de América del Sur, Sierras Pampeanas, Argentina. Journal of Iberian Geology 27, 23–41.
Rapela, C.W., Fanning, C.M., Baldo, E.G., Dahlquist, J.A., Pankhurst, R.J., Murra, J.A., 2005. Coeval S- and I-type granites in the Sierra de Ancasti, Eastern Sierras Pampeanas, Argentina. In: Pankhurts, R.J., Veiga, G.D. (Eds.), Gondwana 12: Geological and Biological Heritage of Gondwana. Academia Nacional de Ciencias, Córdoba, p. 307.
Rapela, C.W., Pankhurst, R.J., Casquet, C., Fanning, C.M., Baldo, E.G., González-Casado, J.M., Galindo, C., Dahlquist, J., 2007. The Río de la Plata craton and the assembly of SW Gondwana. Earth-Science Reviews 83, 49–82.
Rossi de Toselli, J., Toselli, A.J., Willner, A., Medina, M.E., 1987. Geotermobarometría de granate-biotita-cordierita en los gneises de alto grado entre las regiones de Cafayate y Colalao del Valle, Sierra de Quilmes, Argentina. In: 10° Congreso Geológico Argentino 3, 25–30.
Rossi, J.N., Toselli, A.J., Saavedra, J., Sial, A.N., Pellitero, E., Ferreira, V.P., 2002. Common crustal source for contrasting peraluminous facies in the early Paleozoic Capillitas Batholith, NW Argentina. Gondwana Research 5 (2), 325–337.
Rubatto, D., Williams, I.S., Buick, I.S., 2001. Zircon and monazite response to prograde metamorphism in the Reynolds Range, Central Australia. Contributions to Mineralogy and Petrology 140, 458–468.
Rudnick, R.L., Gao, S., 2003. Composition of the continental crust. Treatise on Geochemistry 3, 1–64.
Sawyer, E.W., 1999. Criteria for the Recognition of partial melting. Physical Chemical Earth (A) 24 (3), 269–279.
Sawyer, E.W., 2008. Atlas of Migmatites. Canadian Mineralogist: Special Publication 9. NRC Research Press, 371 pp.
Siivola, J., Schmid, R., 2007. List of Mineral Abbreviations. Recommendations by the IUGS Subcommission on the Systematics of Metamorphic Rocks. www.bgs.ac.uk/SCMR SCMR website.
Simpson, G.D.H., Thompson, A.B., Connolly, J.A.D., 2000. Phase relations, singularities and thermobarometry of metamorphic assemblages containing phengite, chlorite, biotite, K-feldspar, quartz and H_2O. Contributions to Mineralogy and Petrology 139, 555–569.
Sims, J.P., Ireland, T.R., Camacho, A., Lyons, P., Pieters, P.E., Skirrow, R.G., Stuart-Smith, P.G., Miró, R., 1998. U-Pb, Th-Pb and Ar-Ar geochronology from the southern Sierras Pampeanas, argentina: implications for the Palaeozoic tectonic evolution of the western Gondwana margin. In: Pankhurst, R.J., Rapela, C.W. (Eds.), The Proto-Andean Margin of Gondwana. Geological Society of London, Special Publication, 142, pp. 259–281.
Spear, F.S., 1993. Metamorphic Phase Equilibria and Pressure-temperature-time Paths. Mineralogical Society of America, Washington, 799 pp.
Spear, F.S., Kohn, M.J., Cheney, J.T., 1999. P-T paths from anatectic pelites. Contributions to Mineralogy and Petrology 134, 17–32.
Steiger, R.H., Jäeger, E., 1977. Subcommission on geochronology: convention on the use of decay constants in geo- and cosmochronology. Earth and Planetary Science Letters 36, 359–362.
Steenken, A., Wemmer, K., López de Luchi, M.G., Siegesmund, S., Pawlig, S., 2004. Crustal provenance and cooling of the basement complexes of the Sierra de San Luis: an insight into the tectonic history of the proto-Andean margin of Gondwana. Gondwana Research 7, 1171–1195.
Steenken, A., Siegesmund, S., López de Luchi, M.G., Frei, R., Wemmer, K., 2006. Neoproterozoic to Early Palaeozoic events in the Sierra de San Luis: implications for the Famatinian geodymamics in the Eastern Sierras Pampeanas (Argentina). Journal of the Geological Society of London 163, 965–982.
Steenken, A., Siegesmund, S., Wemmer, K., López de Luchi, 2008. Time constraints on the Famatinian and Achalian structural evolution of the basement of the Sierra de San Luis (Eastern Sierras Pampeanas, Argentina). Journal of South American Earth Sciences 25, 336–358.
Toselli, A.J., 1990. Metamorfismo del Ciclo Pampeano. In: Aceñolaza, F.G., Miller, H., Toselli, A.J. (Eds.), El Ciclo Pampeano en el noroeste Argentino. Serie Correlación Geológica, vol. 4. Universidad Nacional de Tucumán, San Miguel de Tucumán, pp. 181–197.
Toselli, A.J., 1992. El magmatismo del noroeste argentino. In: Reseña sistemática e interpretación. Serie Correlación Geológica, vol. 8, Tucumán, 243 pp.
Toselli, A.J., Aceñolaza, F.G., Rossi de Toselli, J.N., 1986. A Proposal for the Systematization of the upper Precambrian-lower paleozoic basement in the Sierras Pampeanas, argentina. Zentralblatt für Geologie und Paläontologie I (9/10), 1227–1233.
Toselli, A.J., Sial, A.N., Saavedra, J., Rossi de Toselli, J.N., Pinto Ferreira, V., 1996. Geochemistry and genesis of the S type, cordierite-andalusite-bearing Capillitas Batholith, Argentina. International Geology Review 38, 1040–1053.
Toselli, G.A., 1983. Petrografía del stock granitoide de Las Juntas y metamorfitas encajantes, Sierra de Ambato, provincia de Catamarca. Revista de la Asociación Argentina de Mineralogía, Petrología y Sedimentología 14 (1/2), 15–24.
Vernon, R.H., 1996. Problems with inferring P-T-t paths in low-P granulite facies rocks. Journal of Metamorphic Geology 14, 143–153.
Vernon, R.H., 2004. A Practical Guide to Microestructure. Cambridge University Press, 594 pp.
Vielzeuf, D., Montel, J.M., 1994. Partial melting of metagreywackes. Part I. Fluid-absent experiments and phase relationships. Contributions to Mineralogy and Petrology 117, 375–393.
Vujovich, G.I., 1994. Geología del basamento ígneo-metamórfico de la loma de Las Chacras, sierra de La Huerta, San Juan. Revista de la Asociación Geológica Argentina 49, 321–336.
Waters, D.J., 2001. The significance of prograde and retrograde quartz-bearing intergrowth microstructures in partially meted granulite-facies rocks. Lithos 56, 97–110.
Willner, A.P., 1983. Evolución metamórfica. In: Aceñolaza, F.G., Miller, H., Toselli, A.J. (Eds.), La Geología de la Sierra de Ancasti. Münstersche Forschungen zur Geologie und Paläontologie, vol. 59, pp. 189–200. Münster.
Willner, A.P., Toselli, A.J., Basán, C., Vides de Bazán, M.E., 1983. Rocas metamórficas. In: Aceñolaza, F.G., Miller, H., Toselli, A.J. (Eds.), La Geología de la Sierra de Ancasti. Münstersche Forschungen zur Geologie und Paläontologie, vol. 59, pp. 31–78. Münster.

Willner, A.P., Lottner, U.S., Miller, H., 1987. Early Paleozoic structural development in the NW Argentine basement of the Andes and its implication for geodynamic reconstructions. In: McKenzie, G.D. (Ed.), Gondwana 6: Structure, Tectonics and Geophysycs. American Geophysical Union Monograph, vol. 40, pp. 229–239.

Willner, A.P., Miller, H., Jezek, P., 1990. Composición geoquímica del basamento sedimentario-metamórfico de los Andes del NW Argentino (Precámbrico superior-Cámbrico inferior). In: Aceñolaza, F.G., Miller, H., Toselli, A.J. (Eds.), El Ciclo Pampeano en el noroeste Argentino. Serie Correlación Geológica, vol. 4. Universidad Nacional de Tucumán, San Miguel de Tucumán, pp. 161–179.

Wyhlidal, S., Thöny, W.F., Tropper, P., 2007. New experimental constraints on the Na-in-cordierite thermomether and its application to high-grade rocks. Geochimica et Cosmochimica Acta 71 (15), A1129. Suppl. 1.

Wu, C., Zhang, J., Ren, L., 2004. Empirical garnet-biotite-plagioclase-quartz (GBPG) geobarometry in medium- to high- grade metapelites. Journal of Petrology 45 (9), 1907–1921.

Yardley, B.W.D., 1977. An empirical study of diffusion in garnet. American Mineralogist 62, 793–800.

Yardley, B.W.D., 1989. An Introduction to Metamorphic Petrology. Longman Earth Science Series, London, 248 pp.